

Review

Sol-Gel Coating Membranes for Optical Fiber Sensors for Concrete Structures Monitoring [†]

Bárbara R. Gomes ¹, Rui Araújo ¹, Tatiana Sousa ¹ and Rita B. Figueira ^{1,2,*}

¹ Centro de Química, Campus de Gualtar, Universidade do Minho, 4710-057 Braga, Portugal; barbara.sgomes11@gmail.com (B.R.G.); ruiFilipe.a@gmail.com (R.A.); tatianagsousa@hotmail.com (T.S.)

² Vasco da Gama CoLAB, Rua Roberto Frias, 4200-465 Porto, Portugal

* Correspondence: rita.figueira@vgcolab.com

[†] This paper is dedicated to the memory of Professor Carlos J. R. Silva who passed away suddenly on 27 August 2020.

Abstract: The use of advanced sensing devices for concrete and reinforced concrete structures (RCS) is considered a rational approach for the assessment of repair options and scheduling of inspection and maintenance strategies. The immediate benefits are cost reduction and a reliable prevention of unpredictable events. The use of optical fiber sensors (OFS) for such purposes has increased considerably in the last few years due to their intrinsic advantages. In most of the OFS, the chemical transducer consists of immobilized chemical reagents placed in the sensing region of the optical sensor by direct deposition or by encapsulation in a polymeric matrix. The choice of the support matrix impacts directly on the performance of the OFS. In the last two decades, the development of OFS functionalized with organic–inorganic hybrid (OIH) sol–gel membranes have been reported. Sol–gel route is considered a simple method that offers several advantages when compared to traditional synthesis processes, allowing to obtain versatile materials with unique chemical and physical properties, and is particularly valuable in the design of OIH materials. This review will provide an update of the current state-of-the-art of the OFS based on OIH sol-gel materials for concrete and RCS since 2016 until mid-2021. The main achievements in the synthesis of OIH membranes for deposition on OFS will be discussed. The challenges and future directions in this field will also be considered, as well as the main limitations of OFS for RCS monitoring.

Keywords: optical fiber sensors; sol-gel; hybrids; sensing membranes; OIH; concrete structures



Citation: Gomes, B.R.; Araújo, R.; Sousa, T.; Figueira, R.B. Sol-Gel Coating Membranes for Optical Fiber Sensors for Concrete Structures Monitoring. *Coatings* **2021**, *11*, 1245. <https://doi.org/10.3390/coatings11101245>

Academic Editor: Tsvetanka Babeva

Received: 1 September 2021

Accepted: 8 October 2021

Published: 13 October 2021

Publisher's Note: MDPI stays neutral with regard to jurisdictional claims in published maps and institutional affiliations.



Copyright: © 2021 by the authors. Licensee MDPI, Basel, Switzerland. This article is an open access article distributed under the terms and conditions of the Creative Commons Attribution (CC BY) license (<https://creativecommons.org/licenses/by/4.0/>).

1. Introduction

Concrete degradation is a complex process that results from physical and chemical reactions between concrete components and their surrounding environment. The corrosion of steel in reinforced concrete structures (RCS) has been widely studied and reported by several authors [1–7], since its premature degradation often results in expensive costs of repair, maintenance, and rehabilitation. To mitigate corrosion in RCS and improve their service life, different approaches—destructive and non-destructive methods—have been developed with the aim of monitoring both existing and new structures. Destructive methods provide information about the corrosion process [3,8]. Nevertheless, some constraints exist due to the heterogeneity of RCS and to the fact that the structures are limited to sampling [3]. On the other hand, the non-destructive methods (NDM) provide fast and real-time information about the entire structure. NDM enable the detection of the corrosion state of steel in concrete and the main causes of the reinforcement corrosion [3] as they allow to check active cracks, determine moisture ingress [9], the strength gain [10], as well as the chloride ions (Cl[−]) ingress [11].

The steel reinforcement in concrete is naturally protected by the high alkalinity of the concrete (pH > 12.5) that promotes the formation of a passive film on its surface during the curing process. This oxide layer can be influenced by the steel substrate, as well as

the external environment [12]. In 2016, Alhozaimy et al. [13] studied the consequences of changing the oxygen concentrations on the quality of the passive films formed on the surface of steel rebars in RCS. It was shown that to develop a strong and stable passivation layer, which in turn would lead to low corrosion rates, a suitable amount of oxygen in the surrounding environment of the rebar and the concrete specimen must be present during the initial curing period. To prove that the authors left the specimens unsealed in the laboratory under ambient conditions, with free oxygen supply, completely sealed concrete specimens with no oxygen available were considered for comparison purposes and developed a weak passive layer, exhibiting higher corrosion rates [13].

Generally, in aggressive environments such as marine and industrial, a decrease in structural durability occurs. Concrete carbonation and aggressive species, such as Cl^- , induce the corrosion process by destroying the passive layer on the steel surface [14]. The carbonation process results from the reactions between atmospheric CO_2 and alkaline components of concrete. During concrete carbonation, the initial pH values may decrease to values between 6–9. The pH of concrete is influenced by the CO_2 and depends on the humidity and the temperature that, in specific conditions, may accelerate the entire process. Cl^- can penetrate the passive layer and when they exceed the chloride threshold value (CTV), the steel depassivation process begins, leading to the corrosion of reinforcing bars [4,14]. In 2007, Song et al. [14] determined this critical value to be equal to 1.2 kg m^{-3} . Additionally, they also assumed that by the time the Cl^- content reached 2.4 kg m^{-3} , the passive film no longer existed.

The products resulting from the corrosion of reinforcement in concrete—expansive oxides—occupy a higher volume than the initial uncorroded rebar, as shown in Figure 1. These oxides promote the formation of expansive forces in concrete and, as a consequence, induce cracking and with time to concrete detachment [3]. The evolution of the corrosion process associated with a decrease in strength and ductility of reinforcement, in extreme cases, may lead to the collapse of the structures.

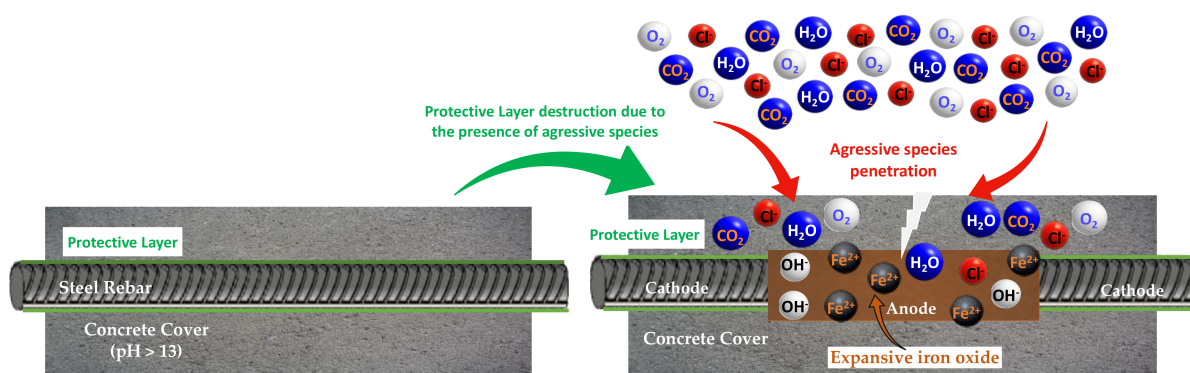
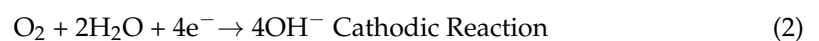


Figure 1. Electrochemical corrosion process on the concrete surface [7].

Concrete corrosion is an electrochemical process on the steel surface, based on two reactions—anodic (Equation (1)) and cathodic (Equation (2))—that take place in different locals of the rebar.



To minimize or avoid corrosion of the concrete reinforcement, a suitable monitoring system is required. Optical fiber sensors (OFS) have proven to be an interesting and promising alternative in comparison with the conventional electrochemical ones. The main advantages of OFS are the robustness, small size, immunity to electromagnetic interference, high sensitivity, and resistivity to corrosion [15,16]. The development of functionalized

OFS coupled to organic–inorganic hybrid materials (OIH) has shown promising and very interesting properties [17,18].

OIH are a new generation of multifunctional materials with a broad spectrum of useful properties and a diversity of applications [19]. They have several advantages, since they are chemically inert and resistant to thermal, photochemical, and biodegradation [20]. Moreover, OIH materials enable the incorporation of different components that introduce complementary functions to the material such as UV protection [21], anti-reflection [22], moisture resistance [23,24], corrosion inhibition [25], and adhesion protection [26]. Sol–gel is one of the most effective synthetic methods to produce OIH materials using organic solvents at mild temperatures [19,27]. It is also recognized as green, low-cost, and a versatile route [28]. Therefore, it is the main technology implemented for the synthesis of OIHs. The precursors and the synthesis conditions can be tuned, allowing to obtain a product with suitable physicochemical properties according to the required application. Additionally, sol-gel method is a versatile process that enables to adjust the porosity of the OIH matrix allowing the incorporation of sensitive species, such as chemosensors, into the OIH matrix [29]. The versatility of the sol-gel method [28,30,31] allows adjusting and controlling several parameters such as precursors, matrix porosity, curing time, and temperature of the OIH, making them a supporting membrane with suitable and interesting properties and the ability to host species for a given analyte [18,19,29].

Chemosensors are organic receptor molecules that selectively interact with a specific analyte, providing chemical information through the generation of detectable signals. Chemosensors use molecular recognition mechanism for recognition of an analyte, allowing the occurrence of the signal transduction. The signal produced may be based on the principles of fluorescence [32] or absorbance [33]. These types of molecules add to the OIH membrane's extra optical and electrical properties. In this context, it is easy to comprehend that these new OIH materials show auspicious properties for application as supporting films in optical sensors area, such as fiber sensor devices. OFS based on OIH materials doped with chemosensors are a promising alternative due to the high selectivity of these molecules combined with the accuracy of the optical sensors [18]. These molecules may be introduced within the OIH matrices after polymerization, allowing obtaining OIH membranes with tuned functions.

This review is focused on the main achievements in the synthesis of OIH membranes for deposition on OFS. The OFS based on OIH sol-gel membranes for pH, Cl^- , and moisture monitoring in concrete developed in the last years i.e., since 2016 until mid-2021, will be reviewed. The challenges and future directions in this field will also be debated, as well as the main limitations of OFS for RCS monitoring.

2. Optical Fiber Sensors (OFS)

2.1. Fundamentals

The first patents focused on the preparation and application of OFS appeared in the 1960s [1]. Since then, the developments in this particular area have been quite noteworthy [2–6]. The progress achieved is mainly related to the use of optical fibers by the telecommunications companies whose investigation and development made it possible to manufacture high quality fibers with a low production cost [1]. The widespread use of these type of sensors is also due their advantages, namely, the low installation costs, robustness, immunity to electromagnetic interferences, chemical inertia, thermal resistance, and wide bandwidth [1].

Generically, a device based on an OFS has a source, a modulator, a detector, and an electronic processing unit that makes the conversion of an optical signal in an electric one [7]. Figure 2 shows a schematic layout of an OFS.

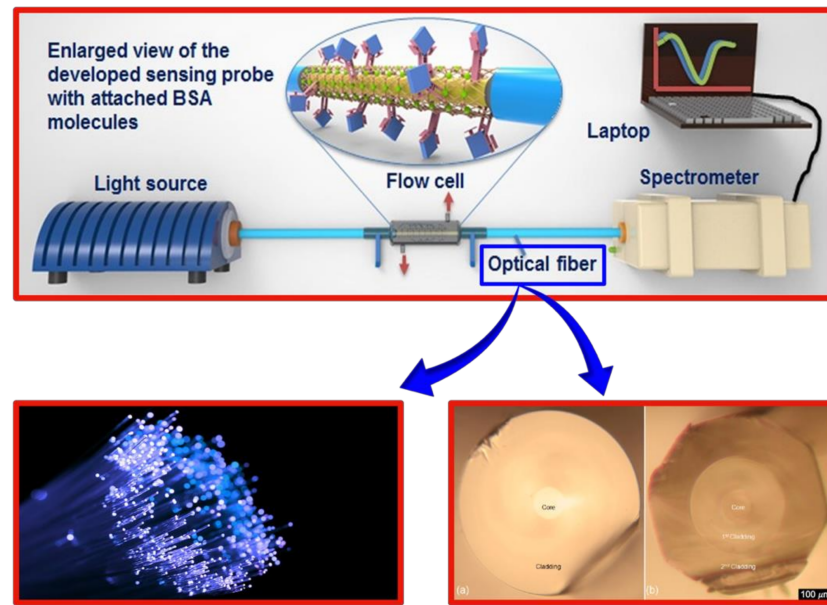


Figure 2. Layout of an OFS. Right side shows microscopic cross-section images of the double-coated optical fibers. (a) in the passive fiber the transition from the inner to the outer cladding occurs at a lower RI; (b) octagonal cross section of the second cladding of the active doped fiber [8,9].

Generically, OFS may be classified in two main classes, namely the intrinsic and extrinsic ones. In an extrinsic sensor, the fiber itself is used as a mean of transportation of light from the source to the detector and the modulation of the signal occurs outside the fiber (Figure 3) [10]. In an intrinsic one, the light is also transported from the source to the detector through the fiber, however the modulation of the signal occurs inside the fiber (Figure 3) [10]. The conditions of the surrounding environment will cause changes in the physical properties of the fiber which will induce changes in the properties of the transmitted signal, such as reflection and refraction [11,12].

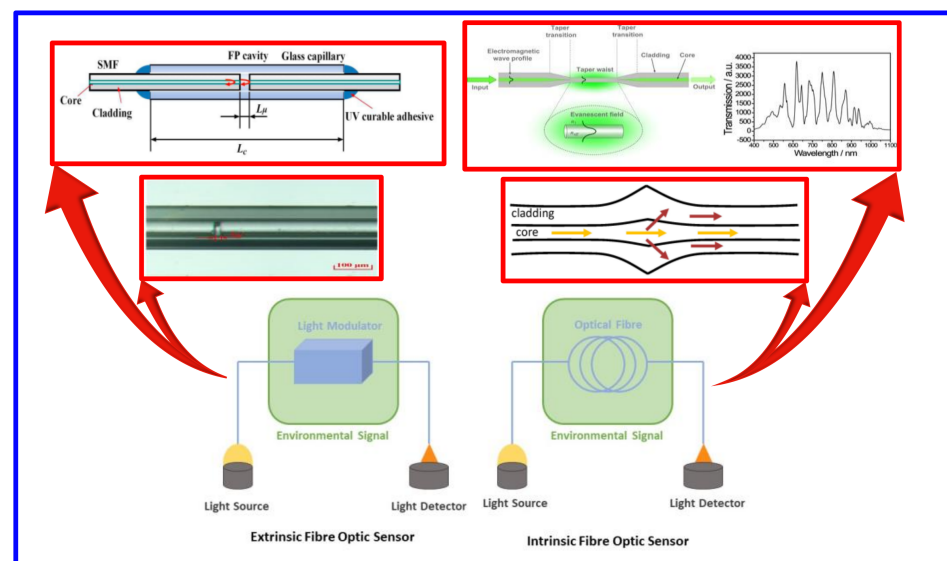


Figure 3. Typical configurations of chemical OFS. Extrinsic sensors, in which fiber is used to direct light and intrinsic sensors, in which the sensor phase modifies the transmission characteristics of the fiber. The sensor membrane can be placed on the tip of the fiber or to the side; part of the coating can be removed and leave the fiber core exposed to the chemical interaction medium [13–16].

The development of OFS has expanded in recent years, favoring advances in different areas such as telecommunications [17,18], materials chemistry [19,20], microelectronics [21–23], and nanotechnology [24–26]. Focusing on the area of chemistry, most of the existing OFS are based on transduction principles such as fluorescence [27–30] or absorbance [31,32]. In the mentioned cases, the analytical response is achieved by changing the optical properties of a fixed recognition agent on a solid support due to the interaction with the species to be determined.

Chemical sensors are generically defined as devices that convert chemical information, in real time, into a measurable analytical signal [33,34]. They contain two basic functional units: a recognition element (receiver) and a transduction mechanism. The receptor can be based on three principles: physical, chemical, or biochemical. The transduction mechanism may be classified as optical, electrochemical, piezoelectric, and thermal [33]. Figure 4 schematizes examples of the aforementioned mechanisms.

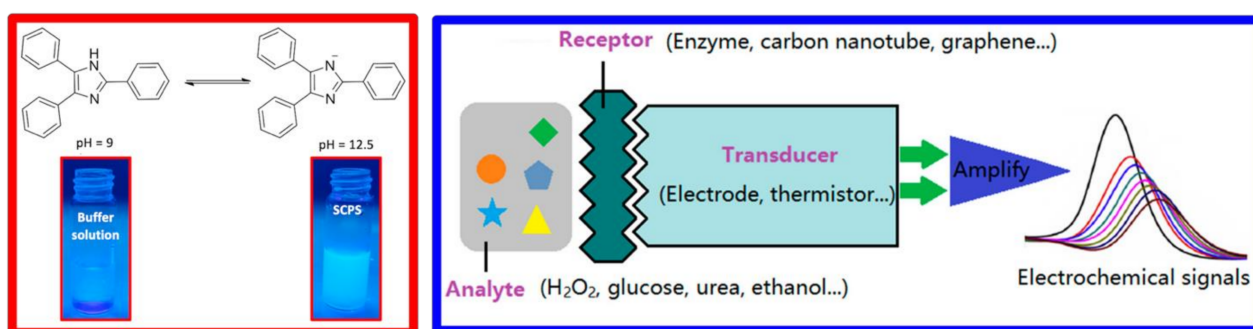


Figure 4. Chemical sensors and respective mechanisms. Right side show the fluorescence of the samples irradiated under 365 nm. Left side show the signal obtained [35,36].

Optical sensors, or optrodes, are chemical sensors where electromagnetic radiation is used to generate analytical signals in the transducer element. They can be based on optical principles such as absorbance, reflectivity, luminosity, and fluorescence (Figure 4), covering different regions of the spectrum (ultraviolet (UV), visible, infrared (IR), near infrared (NIR)), not only to measure light intensity, but also other intensity-related properties such as RI, scattering, diffraction, and polarization. In this type of sensor, an optical fiber is usually incorporated to transmit the electromagnetic radiation to a sensitive area in direct contact with the sample, or directly from the sample [34]. Distal type sensors are the most common ones, where the indicator is fixed at the tip of a simple or forked optical fiber. Alternatively, the chemical sensor can be immobilized along a portion of the optical fiber core, creating an evanescent field sensor. Figure 5 shows the light-matter interaction on the surface of a biosensor. The biosensor consists of a metallic nanostructure supporting a plasmonic resonant mode integrated into the optical fiber [37]. The analyte–receptor molecule binding induces the shift of the maximum reflectance peak to longer wavelengths (right), with no change in intensity.

Bragg network sensors are characterized by the periodic modification of the RI of the optical fiber core due to exposure to an intensity pattern produced by ultraviolet (UV) radiation interference [38–41]. The incident radiation is transmitted and reflected. Fiber Bragg gratings (FBGs) selectively reflect radiation with a certain wavelength, determined by the Bragg condition (Equation (4)) [38,42–45]. All signals with different Bragg wavelengths are transmitted unchanged [40].

$$\lambda_B = 2n_{\text{eff}}\Lambda \quad (4)$$

λ_B is the Bragg wavelength, n_{eff} is the effective refractive index of FBGs, and Λ is the grating period. The Bragg wavelength is sensitive to external disturbances such as temperature and voltage variations [39,46]. When the network is subjected to external disturbances, the period of the network changes and the Bragg wavelength changes linearly [38,39,45].

Therefore, monitoring the deviation of the Bragg allows the determination of parameters of interest such as voltage, temperature, and flux.

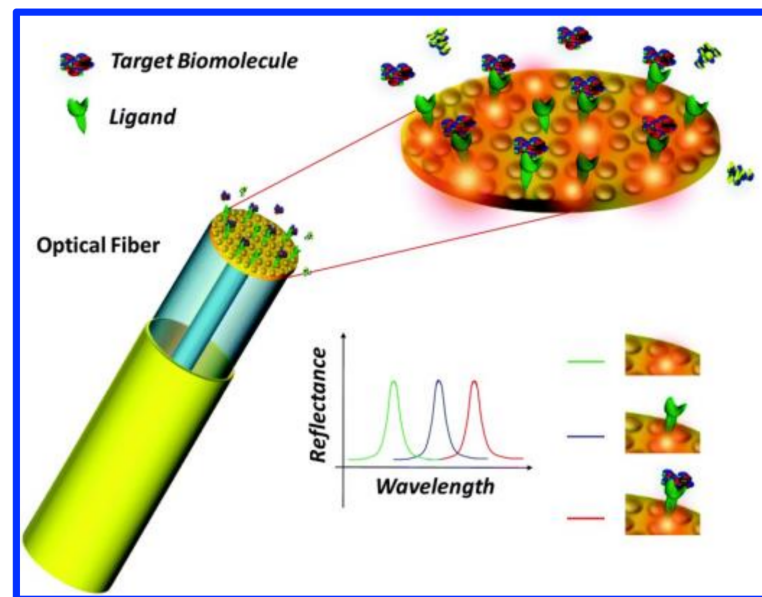


Figure 5. Distal type sensors. Adapted with permission from [37] Copyright 2015 © Royal Society of Chemistry.

FBGs show highly promising alternatives for structural health monitoring (SHM) since it allows to combine intrinsic and OFS features. FBGs have small dimensions, immunity to electromagnetic interference, as well as high linearity, sensitivity, and multiplexing capacity, and may be incorporated into several types of structures including existing and new ones [38,42,47]. Figure 6 shows the layout of FBGs sensor.

Commonly, in an optical sensor, the chemical transducer consists of immobilizing chemical reagents placed in the optical sensor zone by direct deposition or encapsulation in a polymer or OIH sol-gel matrix. The choice of polymer support can influence sensor performance, i.e., its selectivity and response time (RT), and is controlled by parameters such as mechanical stability, analyte permeability, and reagent immobilization capacity [34].

Due to its simplicity and versatility, sol-gel technology is widely used in the development of OFS [19,48–52]. In this process, porous thin films doped with different chemical and biochemical species with sensory abilities, for a given analyte, are easily obtained at room temperature, allowing final structures with mechanical and thermal stability and suitable optical properties [34]. The use of OFS was reported in the measurement of several properties such as pressure [53], temperature [54], strain [55], chemical changes [56], humidity [57], pH [58], and others [59].

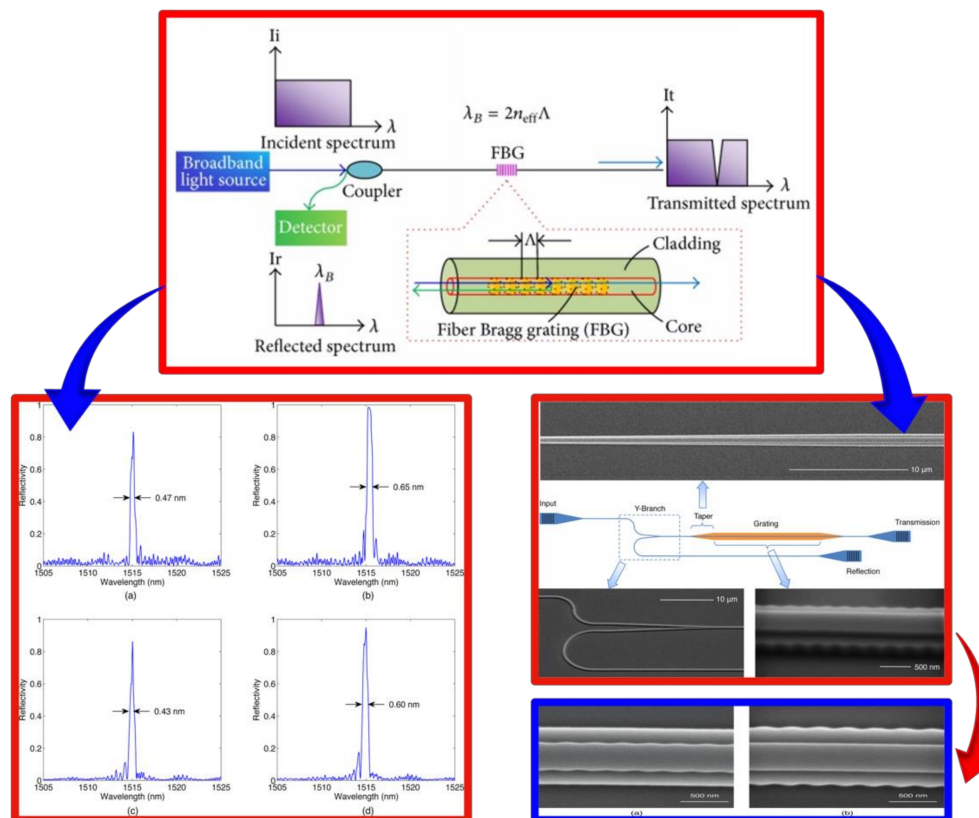


Figure 6. Layout of FBGs sensor. Left: Reflection spectra obtained using Bragg gratings on ridge waveguides (a,b) ridge grating, (c,d) slab grating. Adapted with permission from [39] Copyright 2015 © Royal Society of Chemistry. Right: The two configurations show similar performance but with a slight difference in bandwidth. SEM images of each of the FBG sensor components with emphasis on the top view ones of Bragg gratings (a) grating on ridge and (b) grating on slab [60].

2.2. Applications

In the past 25 years [59], the development of OFS has been increasing due to the need to implement techniques that allow an evaluation and monitoring in real time several parameters. This need is interesting in a wide range of fields and construction is not an exception, aiming to ensure the integrity of RCS. The use of OFS has proved to be a remarkable alternative due to its intrinsic properties, high sensitivity, and resistance to corrosion [61].

The application of OIH materials in OFS is promising due to the high stability of the matrix, the wide flexibility in sensor specificity, and the control of porosity and surface properties (hydrophilic/hydrophobic balance). The development of OFS functionalized with OIH materials has already been reported for application in several fields, including biomedical [52], civil engineering [28,62–64], and environment [48,56,65].

Bhardwaj et al. [66] reported the development of an OFS for pH detection with different indicators, namely bromophenol blue, cresol red, and chlorophenol red, achieving a pH range between 2 and 13. A shift in resonance wavelength towards blue in alkaline solutions (-0.93 nm/pH) and a shift in resonance wavelength towards red in acidic solutions (1.02 nm/pH) were found. Pathak and Singh [67] reported another type of OFS for pH monitoring with three indicators, namely bromothymol blue, cresol red, and chlorophenol red. A pH range between 4 and 13 and a sensitivity of 0.49 dBm/pH was reported. In another field of application, Liu et al. [68], developed a fiber optic pH sensor aiming to detect ammonia in water. The sensor with the thicker silica coating showed higher sensitivity compared to the sensor with the thinner silica coating (0.131 nm/ppm and 0.069 nm/ppm, respectively). However, further refinement of the experimental results

allowed the sensor to achieve a sensitivity of 2.47 nm/ppm. Kant et al. [69] reported the development of an OFS for the detection of caffeine integrating reduced graphene oxide nanohybrid membranes on chitosan modified silica membrane. The sensor features a detection limit of 1.994 nM and operates over a concentration range between 0 and 500 nM with a RT of 16 s. Despite the wide spectrum of applications and publications reported, the development of OFS functionalized with OIH materials is still at an early stage.

3. OFS for Durability Monitoring of Concrete and Reinforced Structures

The premature degradation of civil engineering structures such as bridges, tunnels, and dams, in contrast to the estimated lifetime and the high maintenance costs, has led to the need to develop and implement a set of methods to assess the current state of the structures in real time. SHM in concrete has been widely reported by several authors since allows monitoring several structural and environmental parameters by implementing a set of strategies for diagnosis, prevention and early identification of possible factors that induce concrete corrosion namely cracks, deformations, pH, temperature, moisture, and Cl^- content [39,70–73]. Additionally, SHM enables optimizing decision-making to avoid catastrophic failures in civil structures [72].

Monitoring of structures is mainly carried out by piezoelectric [74–76], strain [77,78], and OFS sensors [79–82]. The OFS are based on interferometric principles (Fabry-Perot and MZI) and optical (Bragg Fibers) or stimulated (Brillouin) dispersion principles [83,84].

OFS are promising in new, existing, or repaired concrete structures as they can detect a decrease in performance or the appearance of failures and pathologies [61]. However, they have not yet achieved all the desirable properties. The monitoring and identification of concrete pathologies are a complex process as structures are exposed to a variety of physical (temperature), chemical (pH and Cl^- content), and mechanical (cracking and deformation) degradation processes. On the other hand, the heterogeneity of concrete structures makes it necessary to obtain essential information, i.e., the exact location of cracks [70,85,86]. Rossi and Le Maou [87] demonstrated how a crack can cause the breakage of an optical fiber and therefore total elimination of the transmitted signal. Moreover, the incorporation of OFS into concrete structures may result in small cracks ($<1 \mu\text{m}$), inducing the ingress of moisture or Cl^- [72]. The cracks compromise the integrity, permeability, and corrosion resistance of concrete structures [72,88].

OFS have a dual sensitivity to temperature and strain, requiring the separation of the respective parameters. The coating polymer used in optical fibers also absorbs some strain, which may lead to inaccurate structural strain readings [89]. In recent decades, the development of OFS functionalized with OIH sol-gel membranes has proven to be a promising alternative for SHM as it allows the assessment of different parameters, i.e., pH, moisture, and Cl^- . However, leaching of the doped species and resistance reduction was observed when applied to fresh concrete [34,50]. Therefore, this type of OFS requires suitable coatings with resistance to the adverse conditions and to the fresh concrete pH [72]. Moreover, the long-term stability of the OFS is conditional, since chemical and mechanical changes in concrete modify the properties of the optical fiber [86].

3.1. OFS for pH Monitoring of Concrete Structures

pH measurement is essential in fields of science, such as chemistry [90], environment [91–93], and biomedical [94–98]. The pH of a solution can be determined quickly by using indicator paper or glass electrodes. Both have advantages and disadvantages. The indicator paper only provides an approximate value on the Sorenson scale and not the exact numerical value, while glass electrodes have numerical and accurate values [99,100]. Despite this, glass electrodes may suffer from poor performance with low ionic strength solutions. Advances in modern electrochemical sensor technologies have reached high development in the field of environmental pollution control, and in biological and industrial applications. In such fields, conventional glass electrodes have been widely used, however there are still some limitations in specific applications. For example, it is difficult to use

the configuration of glass sensors in the biomedical area in vivo, clinical, or food monitoring due to glass damage, size, and deformability limitations [94,101]. To overcome the disadvantages of the glass bar, other alternatives were explored, such as the incorporation of structures with metal oxide as an active component and promising materials for new pH sensors. A pH response was considered for certain types of electrically conductive and semiconductor oxides [102–105] i.e., platinum, iridium, ruthenium, osmium dioxide, titanium, palladium, tin, zirconium, lead, rhodium oxides [106–111]. Iridium, ruthenium, and titanium oxides have been widely used in several applications, particularly in pH detection due to their fast response, chemical stability, high durability, and conductivity. Moreover, they can be used at high temperatures and pressures, and in aggressive environments [112–115]. Nevertheless, besides their cost, iridium oxide have other disadvantages, such as the appearance of a different oxide states leading to deviations and hysteresis in measurements [101]. In comparison with other metal oxides, ruthenium oxide has unique properties such as including thermal stability, excellent corrosion resistance, high sensitivity, and low hysteresis and resistivity [116].

In order to advance the current state of the art, new OIH have been synthesized and doped with imidazole derivatives since they are a promising alternative for pH monitoring [35,117,118]. These compounds were widely disseminated about 20 decades ago, but the first synthesis was performed by Heinrich Debus in 1858 [119]. Imidazole is an organic, polar, and amphoteric compound with an aromatic heterocyclic structure. Thereby, they are grouped into a class of heterocyclic compounds since they have a similar ring structure with different substitutes and are the constituents of some substances, namely histamine, histidine, biotin, nuclei acid, and alkaloids [120–122]. Imidazole derivatives are promising probes for pH detection due to the amphoteric nature of their heterocyclic ring, since they can function as selective anions or cations, allowing for the recognition of several analytes [35,123]. Imidazole derivatives can be protonated or deprotonated depending on the pH [35].

Among the several types of sensor technologies available, the use of smart sensors and the industrialization of wireless sensor networks have attracted considerable attention in this research field [124–126]. Table 1 shows the most relevant optical sensors used for pH monitoring in different conditions and environments. It indicates the type of sensor, i.e., colorimetric or fluorimetric, the precursors and reagents used, the detection range, the sensitivity, and the RT. Table 1 includes the information reported in the last few years, i.e., from 2016 to mid-2021, focused on the study of OFS for pH monitoring based on sol-gel materials applied on concrete or highly alkaline environments (pH > 12). Knowing that the pH value of the healthy concrete pore solution is above 12.5 (and may fall down to values between 6 and 9 when carbonated) [50,127], it is possible to assess the application of the studies reported in Table 1.

Table 1. pH sensors applied to concrete.

Type of Sensor	Precursors/Reagents	Detection Range	Sensitivity	RT	Year	Ref.
Colorimetric	TEOS, cresol red, chlorophenol red and bromophenol blue	2–13	1.02 nm/pH −0.93 nm/pH	NR	2017	[66]
Ratiometric	D4 hydrogel, EtOH, Thymol blue, CdSe and ZnCdSe / ZnS QDs and toluene	>12.5	NR	2 days	2020	[128]
Fluorimetric	Naphth-AlkyneOMe, PVA, DMSO, Poly(vinyl alcohol) and H ₂ O	10.25–13.5	NR	100 s	2021	[129]
	TEOS, SiO ₂ , EtOH, HCl, HAuCl ₄ and Au-SiO ₂	8–12.5	10.08 % T/pH 19.90 % T/pH 13.40 % T/pH	3 min 16 s 19 s	2021	[27]

Table 1 shows that most of the sensors reported were fluorimetric. The one with the shortest RT—16 s—was an optical fluorimetric sensor reported by the authors Lu et al. in 2021, with a pH detection range between 8 and 12.5. A sensor for pH values above 12.5 was reported and was a ratiometric optical one.

As mentioned above, the pH value in considered healthy concrete structures is above 12.5. Analyzing the articles reported in Table 1, it can be highlighted that the detection limit is not reported, so it can only be predicted based on the detection interval. Thus, all methods used in pH monitoring, except for membrane sensors and fluorescent dyes for analytes, show a detection interval within the values of interest. Overall, any method mentioned in the Table 1 is suitable for pH monitoring in concrete structures. It should be noted that pH values below 9 in concrete and RCS are worrisome, and the cause of such variation should be investigated and mitigated to avoid further pathologies and deterioration.

3.2. OFS for Chloride Ions Detection

The detection and monitoring of chloride ion (Cl^-) concentration plays an important role in several aspects, including human health [130–132], industrial process control [133], wasted water management [134], drinking water quality control [135,136], and corrosion forecasting of RCS [137–139]. There are several available methods for measuring Cl^- concentration, including electrochemical sensors, OFS [28,140], and Bragg's grating [141,142].

Cl^- is one of the most important indicators for the deterioration of RCS [140,143–146]. In the presence of a critical amount of Cl^- , also known as critical chloride content, reinforcement steel suffers quick localized corrosion, forming pits – pitting corrosion. Pitting corrosion is one of the most common corrosive process in RCS structures in the presence of Cl^- . This corrosion process begins in places where the passivation layer is damaged due to the penetration of aggressive species, i.e., Cl^- [147–149]. Although it does not have a direct and significant impact on the daily operation of a concrete structure, it can affect its structural performance in the medium-long term [150,151]. Corrosion drastically reduces the tensile strength of steel, compromising the load capacity of the structure [50,61,152]. During this process, the passivation layer, i.e., the passive iron oxide film, initially formed on the surface of the steel, is destroyed. In the case of chloride-induced corrosion, the passive film is broken locally. This process comes from the formation of oxides with Fe_2O_3 as the main component and results in the formation of bulky corrosion products, which leads to the early formation of cracks, causing volume expansion and tensile stress in the reinforcement which in turn leads to deformations [140,153,154].

Additionally, structures in the marine environment or exposed to ice/thaw salts are more prone to pitting corrosion. This is particularly true for the ones in the splash zone near the seawater, which is the area close to the air/water interface that suffers from accelerated deterioration due to atmospheric oxygen, water, and Cl^- availability [155–157].

Figure 7 shows the corrosive process in concrete structures in marine environment. The air/water interface induces pitting corrosion by causing the local degradation of the passivation layer. At this site, a small area appears allowing the penetration of O_2 , H^+ or of aggressive species i.e., Cl^- . Throughout the corrosive process, iron oxides are formed. At an early stage, pitting corrosion is difficult to detect since it does not cause significant impacts on the concrete surface.

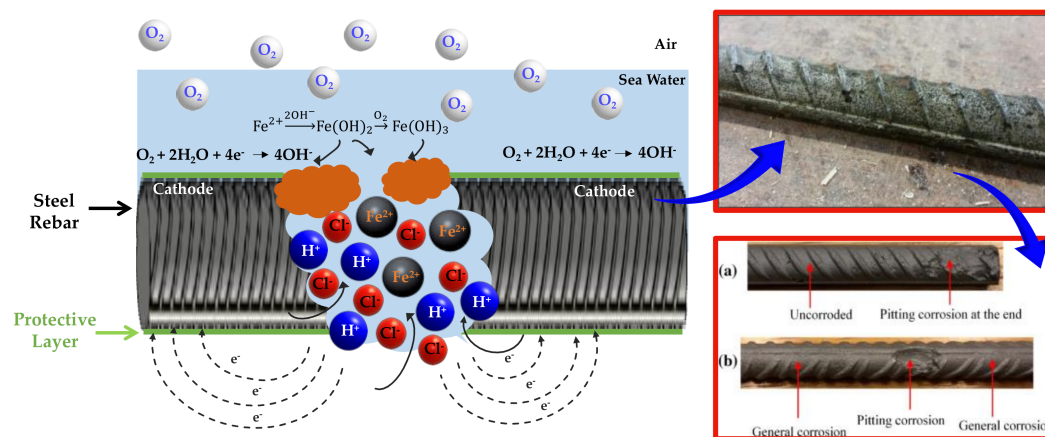


Figure 7. Pitting corrosion [158–160].

Chloride ions threshold value (CTV) refers to chloride ions content that causes visible deterioration in RCS. This may be expressed as the total chloride content as a mass percentage of cement/concrete, or as the molar ratio between $[\text{Cl}^-]$ and $[\text{OH}^-]$. The ratio $[\text{Cl}^-]/[\text{OH}^-]$ reflects the aggressive ions rate for inhibitory ions that lead to the onset of corrosion. Given the risk of chloride pitting corrosion and the inhibitory effect of cement hydration products, this is the reason $[\text{Cl}^-]/[\text{OH}^-]$ has the great advantage of being easy to measure [161].

Table 2 shows some most representative examples of sensors reported for detection of Cl^- . It indicates the type of sensor, i.e., colorimetric, fluorescence, the transducer, the detection limit, the concentration range, and the sensitivity.

Table 2. Some sensors for chloride ion monitoring reported since 2016.

Type of Sensor	Transducer	Detection Limit	Concentration Range	Sensitivity	Year	Ref.
FBG	NR	NR	NR	15.407 nm/RIU 125.92 nm/RIU	2017	[162]
Fluorescence	Lucigenin	0.02 M	NR	NR	2018	[163]
Fluorescence	Chloride-sensitive fluorophore immobilized in a calcium alginate sol-gel	NR	0.045 M–0.45 M	NR	2019	[164]
Fluorescence	Lucigenin	NR	0.02 M–0.06 M	NR	2019	[165]
LPG	NR	NR	NR	9.8 $\mu\text{g}/\text{cm}^2$	2020	[166]

Table 2 shows that most of the sensors reported were based on fluorescence. The sensor reported by Dhouib et al. showed higher concentration range between 0.045 M and 0.45 M using chloride-sensitive fluorophore immobilized in a calcium alginate sol-gel as a transducer. Xiao et al. reported the sensor, which showed smaller concentration range between 0.02 M and 0.06 M using lucigenin as a transducer.

3.3. OFS for Moisture Monitoring

Monitoring humidity is critical in several areas such as civil engineering [167], soils [168], and food packaging [169]. There is a variety of studied, developed, and commercialized electrochemical humidity sensors (HS) that are based on conductivity measures [170–172], humidity sensitive polymers in which the material properties change work as sensors [173,174] and OFS [62,175].

The strength and durability of concrete depends on several factors including temperature and dynamics of moisture transport [176,177]. The properties of concrete material change over time, and these properties (resistance, modulus of elasticity, creep, and shrinkage) are significantly influenced by the hydration heat and moisture content of concrete at an early age [178]. Self-drying due to the temperature of hydrated cement paste causes

an additional decrease in moisture content, at an early age, which influences the properties of young concrete, as well as its medium-long-term behavior [179]. Temperature and high moisture content can also promote deterioration processes. The mechanisms of deterioration of concrete structures (bridges, dams, and buildings), as time goes by, are often related to the moisture and temperature properties of the structures. The moisture present in concrete resulting from seawater, rain, soil, snow, and floods leads to the transfer of high chloride concentrations, resulting in corrosion of reinforced steel bars (Figure 1). This moisture also promotes deterioration and damage resulting from chemical processes, such as carbonation and alkaline aggregate reactions [179]. For example, concrete damage due to ice/defrost is related to moisture transfer.

In these cases, volume changes occur, leading to cracks that may later lead to structural failures [180]. Recent studies have determined that extensive failures in concrete components are related to thermal and humidity variations [181]. These changes and degradation processes are initiated when the relative humidity (RH) level of concrete reaches critical values between 50% and 70% [182].

Therefore, a sensor for continuous monitoring of internal RH and temperature is extremely important during and after construction. When incorporated into concrete, the sensor system can provide key information about its curing process by monitoring indoor temperature and humidity. After being detected, this data can also be integrated into the maturity methods available to predict the resistivity of young concrete [183].

Knowing the strength of concrete at early ages brings great benefits, such as increasing productivity and accelerating construction process by reducing the curing period and consequently removing the formwork. When a concrete structure is put into use, continuous monitoring of internal temperature and humidity will provide information on the process of structural damage due to environmental effects such as ice/defrost cycles, chloride ion diffusion, alkalis–silica reaction, carbonation, and temperature changes.

Current methods for assessing temperature and relative internal humidity, which rely on destructive testing systems, are expensive and slow. In addition, these techniques require special equipment and hard work so that remotes sites gain access to them [182].

Humidity is generally associated with the presence of water in a gaseous state. Therefore, most HS are based on absorption and desorption processes. For OFS, changes in the evanescence field whose RI which are influenced by the absorption or desorption of water molecules are used to determine the RH [184].

Conventional HS (gravimetric, capacitive, and resistive) present some limitations in certain environments that may be in the presence of strong magnetic fields or high temperatures and in which humidity monitoring is vital [185]. When compared to traditional HS, OFS-based HS show several advantages that allow them to operate in harsher conditions.

In the last few years, multiple HS based on optical fibers were reported, mainly FBG [186,187], Fabry-Perot interferometer [188–190] and whispering gallery modes (WGM) [191,192]. FBG based sensors are obtained by coating the surface of the optical fiber with a humidity sensitive material that can change the wavelength of the signal exposed to it. This type of sensor has two major disadvantages i.e., their low sensibility and the fact that its behavior is highly dependent on the temperature, which may lead to measurement mistakes. Regarding Fabry-Perot interferometers, the humidity sensitive coating must be used as an optical cavity. However, the production of this kind of sensors is very complex.

Figure 8 illustrates the typical structure of a Fabry-Perot interferometer which is based on the reflection of light through two reflecting mirrors—fixed and moving—arranged parallel to each other at a small distance. Part of the incident radiation is reflected, and the other part is transmitted into the lens. Interference occurs between the radiation reflected by the mirrors. The black, blue and red arrows (left side) correspond to incident, reflected and transmitted radiation, respectively [193]. Figure 8 right side show the spectra obtained from the scanning Fabry-Perot interferometer traces of the Raman laser emission [194].

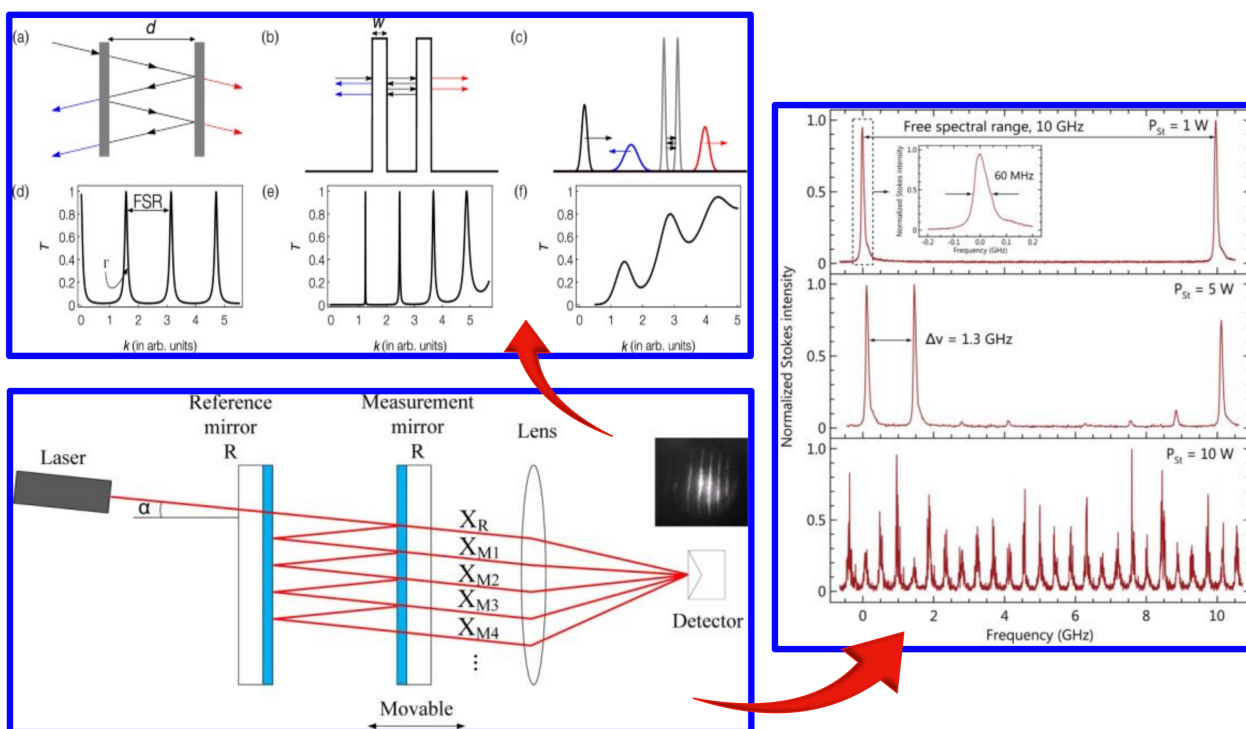


Figure 8. Fabry-Perot interferometers. (a) transmission and reflection of narrow-band light, (b) narrow-band matter-wave through a rectangular double barrier, (c) broad-band Gaussian wavepacket, (d), (e) and (f) correspond to the transmission resonance peaks [193–195].

Finally, whispering gallery modes-based sensors are very delicate regarding their structure, which means that their transportation and application must be performed very cautiously to prevent any damage.

Figure 9 shows the phenomenon of total internal reflection of radiation in WGM along the entire closed concave surface. In successive wave descriptions, radiation losses occur due to absorption and material scattering across the surface. The results illustrate that the blue (before) and red (after) lines represent the WGM transmission line of a resonance shift and associated broadening (left side). The transmission lines before (blue) and after the mode splitting induced by a single (green) or multiple (red) disturbing particles (right side) [196].

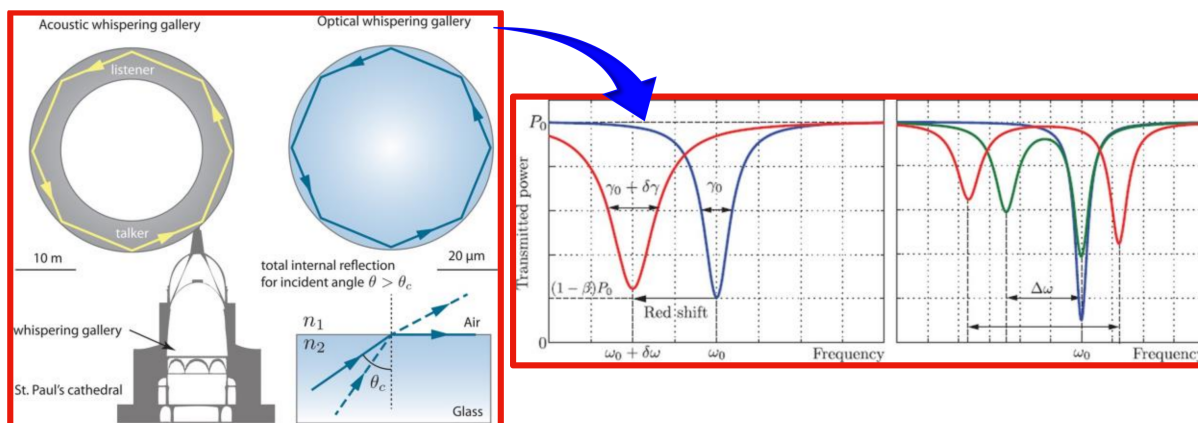


Figure 9. Whispering gallery modes-based sensors. Adapted with permission from [196] Copyright 2015 © The Optical Society.

In 2006, Yeo et al. [197] developed an OFS to measure humidity in concrete. The sensor was developed using a FBG coated with a polyimide. To increase the adhesion between the coating layer and the silica surface, the FBG was treated with 3-aminopropyltriethoxysilane (3-APTS). The coating was achieved through multiple dipping of the FBG in the polyimide, resulting in a total deposition of 20 layers. The sensor was able to detect changes in the moisture content in different samples [197]. Recently, HS based on MZI (Mach-Zehnder interferometer) have also been developed (*vide* Figure 10).

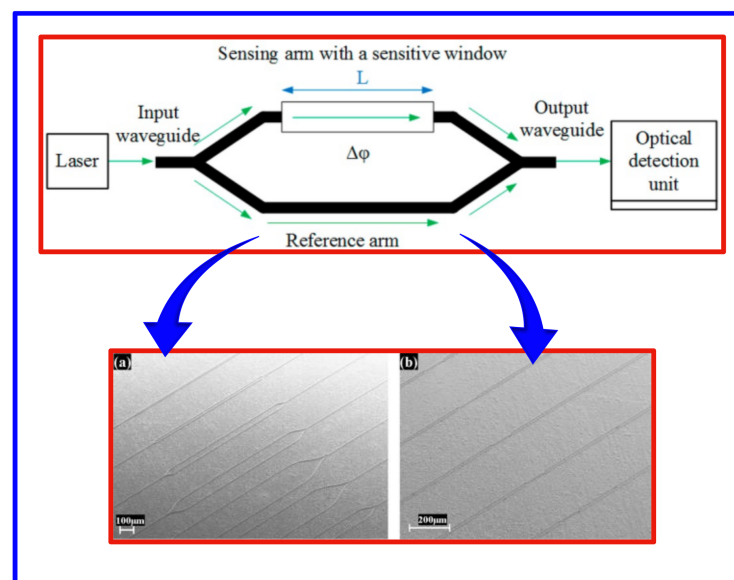


Figure 10. The typical configuration of the MZI structure consists of two waveguides (input and output), a beam splitter (the left Y-function), and a beam combiner (the right Y-function), as well as two straight waveguides between the two Y-functions as the sensor and the reference arms [198]. SEM images illustrate (a) a set of MZI ridge interferometer structures and (b) a set of ridge coupler structures. Adapted with permission from [199]. Copyright 2014 © AIP Publishing.

For instance, Zhang et al. [200] in 2013 developed a sensor capable of measuring RH and temperature at the same time by cascading a photonic crystal fiber-based MZI and a FBG. The sensor was coated with a layer of polyvinyl alcohol that is moisture sensitive. The FBG sensor itself is not sensitive to humidity, however when coated with a sensitive material it becomes one. The coating may absorb the moisture present in the air and therefore dilatate, resulting in some tension on the FBG and the optical fiber that hosts it [201]. The influence of the humidity depends on the type and thickness of the coating and on how tough is the fiber [201]. The production process of the described system must be highly precise so that the simultaneous measurement of temperature and humidity is a reality. The sensor reported presented a range between 30% and 95% of RH [200]. In 2016, Wang et al. [202] developed a HS based on MZI coated with graphite oxide which operation principle is based on light polarization and respective changes in its RI. Graphite oxide was selected because of its RI, which changes accordingly to the RH of surrounding environment. The research team concluded that the sensor showed a maximum sensibility of 0.349 dB/%RH and a detection range between 60% and 77% and a good stability [202]. In 2020, Bian et al. [203] reported a HS composed of calcium alginate hydrogel and a MZI structure. The hydrogel was selected due to its response towards humidity. The authors combined a solution of sodium alginate and calcium chloride to obtain the calcium alginate hydrogel. The sensibility obtained was 0.48346 dB/%RH. The main advantages reported were the simple preparation, non-toxic, and low cost showing good repeatability, stability, and a fast response time [203]. In the last few years, there has been a significant growth in both the technology and uses of HS, since many different industries seek for this type of product [175]. There is a particular interest in sensors based on OF due to the

advantages that they show when compared to electrochemical ones, namely their immunity to electromagnetic interferences and associated cost/benefit relation [204].

Table 3 compiles information from articles focused on the study of resistivity sensors applied to concrete.

Table 3. Resistivity sensors reported since 2016.

Type of Sensor	Precursors/Reagents	Detection Limit	Detection Range	RT	Year	Ref.
Vipulanandan models	NR	NR	17.00 $\Omega \cdot m$ 25.26 $\Omega \cdot m$ 61.24 $\Omega \cdot m$	15–75 min 15–75 min 30–60 min	2018	[205]
Screen-graphed sensor	NR	0.82 $\Omega \cdot m$ 0.61 $\Omega \cdot m$	0.82–9.80 $\Omega \cdot m$ 0.38–9.80 $\Omega \cdot m$	5–7 days	2018	[206]
PCB	Copper tracks, glass-reinforced epoxy laminates	NR	5.8–484.6 $\Omega \cdot m$ 5.7–448.3 $\Omega \cdot m$	NR	2019	[207]
Four electrodes arrangement probe (Wenner type)	NR	NR	10–160 $K\Omega \cdot cm$	NR	2019	[208]

The results obtained from the experiences of the articles mentioned in Table 3 are expressed in different units ($\Omega \cdot m$ and %). For that reason, it is not possible to establish a reference value. Another reason for the lack of a reference value is the fact that there are several types of concrete, i.e., concrete with different constituents that, uniquely, influence resistivity. Table 3 also shows that the number of manuscripts focused on the development of resistivity sensors through the sol–gel method published since 2015 is significantly reduced.

Analyzing Table 3, the most suitable and promising method for resistivity sensor seems to be the screen-graphed sensor, since it is the only manuscript reported that presented a detection limit.

Table 4 shows some examples of optical sensors reported for moisture monitoring. It indicates the precursors and reagents, the RH, the sensitivity, and the response time (RT).

Table 4. Some sensors for moisture monitoring reported in recent years.

Type of Sensor	Precursors/Reagents	RH/%	Sensitivity	RT	Year	Ref.
FBG	Di-ureasil, THF, ICP TES, diamine (Jeffamine 600®) EtOH and HCl	5.0–95.0%	22.2 pm/%RH	NR	2012	[209]
POF	PMMA	30–90 %	NR	6h (50% RH) 31h (90% RH)	2017	[210]
FBG	NMP, ODA, PMDA and PAA	25.0–95.0%	3.38–29.35 pm/%RH	70–110 s 265–436 s	2018	[211]

Table 4 shows that most of the sensors reported were FBG and the one with the shortest RT was the FBG sensor with a RH between 25% and 95% and a sensitivity of 3.38–29.35 pm/%RH. Liehr et al. reported a POF sensor with the shortest RH range.

3.4. Multifunctional OFS for SHM

The development of OFS in civil engineering has increased mainly due to the early degradation of structures such as bridges and dams [61,70,212–215], resulting in an expensive cost of repair and maintenance [49,216–218]. Therefore, OFS enable to monitor and evaluate structural integrity with more accuracy and selectivity, mitigating or preventing structural degradation [61,71,79]. Commonly, OFS are designed to individually monitor parameters such as temperature [64], strain [219,220], pH [66,128,129], moisture [63,197,221], and chloride ion content [28,140]. Variations of those parameters are then transmitted through changes in intensity, frequency, polarization, phase of light, or wavelength. Never-

theless, in recent years, multifunctional OFS have been developed to provide simultaneous information on a set of parameters, which is particularly advantageous to monitor civil structures, considering the number of parameters to be monitored due to the heterogeneity of concrete [200,222,223]. In this case, the application of Bragg gratings in multifunctional OFS is fruitful, mainly because they can monitor several parameters simultaneously, such as temperature, strain, and pH [38,42,47]. Thus, the determination of any change in the respective parameters leads to a change in the wavelength which consequently causes a change in the optical properties i.e., RI and mechanical properties of the materials [224]. Additionally, Bragg gratings provide an absolute, linear, and high-information transmission capacity [225].

The main aim of multifunctional OFS is to monitor, in situ, by a non-destructive method, the corrosion of reinforced concrete structures, the pH, the moisture, and the Cl^- content [226,227]. It is emphasized that Cl^- content and pH are the most important factors in the corrosion of reinforced concrete structures since, at the steel/concrete interface, they can determine the stability or degradation of the passivation film [228]. Besides that, OFS able to determine the Cl^- content tend to be extrinsic [61,229]. To increase the service life of concrete structures, it is desirable to monitor several parameters simultaneously such as pH, humidity, and Cl^- content. Therefore, the development of multifunctional OFS which enable continuous, in situ, and real-time monitoring of mentioned parameters is required.

4. Future and Research Challenges on OIH Sol-Gel Materials for OFS

Corrosion is one of the main problems of modern society that is always linked to high costs, and in extreme situations human lives losses. The development of multifunctional materials may be one interesting alternative and potentially the key to prevent and mitigate the corrosion processes in concrete and RCS. The sol-gel method allows obtaining OIH materials with distinctive properties, since they combine the different characteristics of the organic and inorganic components within the same matrix. Moreover, OIH membranes are innovative materials that allow the incorporation of complementary functions (i.e., UV protection, anti-corrosion, anti-reflection, and anti-fouling).

In the last few decades, the emergence of OFS has overcome most of the shortcomings existing in the conventional sensors due to their intrinsic properties such as small size, corrosion resistance, immunity to electromagnetic interference, and multiplexing capability. The OFS are designed to provide properties not achievable in existing equipment, allowing the acquisition of vital information in real time, ensuring the structural integrity of concrete and RCS.

Regarding all the literature reviewed and discussed through this manuscript, it was shown that the development of OFS functionalized with OIH sol-gel membranes has revealed to be a promising alternative to increase the service life of civil engineering structures. The OFS incorporated in structures, such as concrete exposed to extremely aggressive environments, allow to monitor accurately several physical parameters of the structure's health. Other potential parameters that should be considered are pH, moisture, and Cl^- content to mitigate and/or delay the initiation and development of the corrosion process of concrete and RCS.

The literature shows that the development of OFS functionalized with OIH materials for monitoring the concrete properties is still at an early stage, since most of the reported information is related to the monitoring of physical parameters such as torsion, temperature, displacement, and expansion. From this context emerges the need to develop new OIH sol-gel films/membranes for incorporation in optical fiber systems which can allow monitoring chemical parameters.

In a world that is globally connected, the future of monitoring civil engineering structures is intimately interconnected to smart and automatized systems. OFS are considered a convergence medium between different technologies enabling the production of automatized systems with alarms allowing interventions before real damage occurs. It is undeniable that the monitoring devices that are being developed and reach high projection

will be created based on machine learning, artificial intelligence together with the internet of things (IoT). This will surely lead to the development of extremely smart systems and new concepts. The reflection of this is the well-known concepts of Lab-on-a-Chip and Lab-in-a-fiber [48].

A suitable automatic, multiplexed, and interesting device would be able to monitor important parameters simultaneously for concrete and RCS and at the same time have alarms in case of certain parameters reach threshold values, allowing intervention and repair of the structure to avoid accidents or catastrophes. This mitigates the risk of accidents, victims, as well as the costs involved.

5. Conclusions

The main reasons for early degradation of concrete and RCS are inadequate maintenance, incorrect construction, and failure in continuous monitoring. Exposure to extremely aggressive environments promotes ageing and premature degradation of concrete structures, resulting in high maintenance and repair costs. Preventive and mitigation actions are imperative since the continuous monitoring of structures allow the identification at an early stage of pathologies, favoring the ability to choose among the most suitable and economically feasible methods for each situation. Additionally, monitoring can ensure the projected lifetime, since early identification of the beginning of the corrosion process enables fast intervention, making the whole process more efficient and more cost-effective.

Sol-gel method is a simple, versatile, and environmentally friendly process as it allows obtaining multifunctional OIH materials with unique properties. The application of OIH films/membranes on OFS is promising due different properties such as high matrix stability, wide configuration flexibility in sensor specificity, control of porosity, and surface properties (hydrophilic/hydrophobic balance).

OFS based on OIH materials have a wide applicability in different fields, and civil engineering structures just as attractive as they allow monitoring the relevant parameters such as pH, moisture, and Cl^- content. According to the literature reported through the manuscript, the development of resistivity OFS is still at a very early stage. Besides, pH sensors are the most developed ones as they have a wide field of applications since besides civil engineering field, they are vital in several physiological processes. The most representative pH sensor reported so far is colorimetric, with the smallest pH detection range (i.e., between 2 and 13) and a sensitivity of 1.02 and -0.93 nm/pH for acid and alkaline solutions, respectively. For Cl^- monitoring, the most relevant optical sensors reported were based on fluorescence principle. The sensor that showed the smallest concentration ranged between 0.02 and 0.06 M used lucigenin as a transducer.

OIH materials coupled with optical fiber systems show promising and interesting properties to monitor different parameters in concrete and RCS such as cracks, deformations, strain, temperature, moisture, pH, and Cl^- content. However, further studies are required to minimize and improve the limitations involved, such as the dual sensitivity to temperature and strain and absorption of some strain through the polymeric coating of the optical fiber. Moreover, essential information about the exact local of corrosion is required, as well as the development of suitable coatings to reduce the changes that occur in the properties of the optical fiber due to the aggressive environment.

Author Contributions: Conceptualization, R.B.F.; methodology, R.B.F.; investigation, B.R.G., R.A., T.S.; resources, R.B.F.; writing—original draft preparation, B.R.G., R.A., T.S., R.B.F.; writing—review and editing, B.R.G. and R.B.F.; visualization, R.B.F.; supervision, R.B.F.; project administration, R.B.F.; funding acquisition, R.B.F. All authors have read and agreed to the published version of the manuscript.

Funding: This research was funded by the project “SolSensors—Development of Advanced Fiber Optic Sensors for Monitoring the Durability of Concrete Structures”, with reference POCI-01-0145-FEDER-031220 supported by the Program Budget COMPETE—Operational Program Competitiveness and Internationalization—COMPETE 2020 and the Lisbon Regional Operational Program in its FEDER component and by the budget of FCT Foundation for Science and Technology, I.P. The

authors acknowledge the support of Centro de Química, CQUM, which is financed by national funds through the FCT Foundation for Science and Technology, I.P. under the project UID/QUI/00686/2020 and UID/QUI/00686/2021.

Institutional Review Board Statement: Not applicable.

Informed Consent Statement: Not applicable.

Acknowledgments: Rita B. Figueira acknowledge her husband Hugo Gomes and his sons Francisco Gomes and Manuel Gomes for their support and patience.

Conflicts of Interest: The authors declare no conflict of interest.

Abbreviations

3-APTS	3-aminopropyltriethoxysilane
CTV	Chloride threshold value
DI	Deionized water
EtOH	Ethanol
FBGs	Fiber Bragg Gratings
HS	Humidity Sensors
IR	Infrared
LPG	Long Period Grating
MetOH	Methanol
MZI	Mach-Zehnder interferometer
NDM	Non-destructive methods
NIR	Near Infrared
OFS	Optical fiber sensors
OIH	Organic–inorganic hybrid
PCB	Printed Circuit Board
POF	Polymer Optical Fiber
RCS	Reinforced concrete structures
RH	Relative Humidity
RI	Refraction Index
RIU	Refractive Index Unit
RT	Response Time
SHM	Structural health monitoring
TEOS	Tetraethyl orthosilicate
UV	Ultraviolet
WGM	Whispering Gallery Modes

References

1. Jackson, R.G. *Novel Sensors and Sensing*; Taylor & Francis Limited: Oxfordshire, UK, 2019; ISBN 978-0-367-45431-9.
2. Tabassum, R.; Kant, R. Recent Trends in Surface Plasmon Resonance Based fiber–optic Gas Sensors Utilizing Metal Oxides and Carbon Nanomaterials as Functional Entities. *Sens. Actuators B Chem.* **2020**, *310*, 127813. [[CrossRef](#)]
3. Jiao, L.; Zhong, N.; Zhao, X.; Ma, S.; Fu, X.; Dong, D. Recent Advances in fiber-optic Evanescent Wave Sensors for Monitoring Organic and Inorganic Pollutants in Water. *TrAC Trends Anal. Chem.* **2020**, *127*, 115892. [[CrossRef](#)]
4. Zheng, Y.; Zhu, Z.-W.; Xiao, W.; Deng, Q.-X. Review of Fiber Optic Sensors in Geotechnical Health Monitoring. *Opt. Fiber Technol.* **2020**, *54*, 102127. [[CrossRef](#)]
5. Du, C.; Dutta, S.; Kurup, P.; Yu, T.; Wang, X. A Review of Railway Infrastructure Monitoring Using Fiber Optic Sensors. *Sens. Actuators A Phys.* **2019**, *303*, 111728. [[CrossRef](#)]
6. Liu, X. Evolution of Fiber-Optic Transmission and Networking toward the 5G Era. *iScience* **2019**, *22*, 489–506. [[CrossRef](#)] [[PubMed](#)]
7. Figueira, R.B.; Almeida, J.M.; Ferreira, B.; Coelho, L.; Silva, C.J.R. *Mater. Adv.* in press. **2021**. [[CrossRef](#)]
8. Kaushik, S.; Tiwari, U.K.; Deep, A.; Sinha, R. Two-dimensional Transition Metal Dichalcogenides Assisted Biofunctionalized Optical Fiber SPR Biosensor for Efficient and Rapid Detection of Bovine Serum Albumin. *Sci. Rep.* **2019**, *9*, 1–11. [[CrossRef](#)]
9. Arnaoutakis, G. Novel Up-Conversion Concentrating Photovoltaic Concepts. Ph.D. Thesis, Heriot-Watt University, Edinburgh, Scotland, 2015.
10. Yin, S.; Ruffin, P.B.; Yu, F.T.S. *Fiber Optic Sensors*; CRC Press: Boca Raton, FL, USA, 2017; ISBN 978-1-4200-5366-1.
11. Dislich, H.; Hinz, P. History and Principles of the sol-gel Process, and Some New Multicomponent Oxide Coatings. *J. Non Cryst. Solids* **1982**, *48*, 11–16. [[CrossRef](#)]

12. Elsalamawy, M.; Mohamed, A.R.; Kamal, E.M. The Role of Relative Humidity and Cement Type on Carbonation Resistance of Concrete. *Alex. Eng. J.* **2019**, *58*, 1257–1264. [[CrossRef](#)]
13. Alhozaimy, A.; Hussain, R.R.; Al-Negheimish, A. Significance of Oxygen Concentration on the Quality of Passive Film Formation for Steel Reinforced Concrete Structures during the Initial Curing of Concrete. *Cem. Concr. Compos.* **2016**, *65*, 171–176. [[CrossRef](#)]
14. Song, H.-W.; Kim, H.-J.; Velu, S.; Kim, T.-H. A Micro-Mechanics Based Corrosion Model for Predicting the Service Life of Reinforced Concrete Structures. *Int. J. Electrochem. Sci.* **2007**, *2*, 341–354.
15. Korposh, S.; James, S.W.; Lee, S.-W.; Tatam, R.P. Tapered Optical Fibre Sensors: Current Trends and Future Perspectives. *Sensors* **2019**, *19*, 2294. [[CrossRef](#)] [[PubMed](#)]
16. Correia, R.; James, S.W.; Lee, S.-W.; Morgan, S.P.; Korposh, S. Biomedical Application of Optical Fibre Sensors. *J. Opt.* **2018**, *20*, 073003. [[CrossRef](#)]
17. Weng, Y.; Ip, E.; Pan, Z.; Wang, T. Advanced Spatial-Division Multiplexed Measurement Systems Propositions—From Telecommunication to Sensing Applications: A review. *Sensors* **2016**, *16*, 1387. [[CrossRef](#)] [[PubMed](#)]
18. Alwis, L.; Sun, T.; Grattan, K. Developments in Optical Fibre Sensors for Industrial Applications. *Opt. Laser Technol.* **2015**, *78*, 62–66. [[CrossRef](#)]
19. Gomes, B.; Figueira, R.; Costa, S.; Raposo, M.; Silva, C. Synthesis, Optical and Electrical Characterization of Amino-alcohol Based sol-gel Hybrid Materials. *Polymers* **2020**, *12*, 2671. [[CrossRef](#)] [[PubMed](#)]
20. Sousa, R.P.C.L.; Ferreira, B.; Azenha, M.; Costa, S.P.G.; Silva, C.J.R.; Figueira, R. PDMS Based Hybrid sol-gel Materials for Sensing Applications in Alkaline Environments: Synthesis and Characterization. *Polymers* **2020**, *12*, 371. [[CrossRef](#)]
21. Volkov, P.; Semikov, D.; Goryunov, A.; Luk'yanov, A.; Tertshnik, A.; Vopilkin, E.; Krayev, S. Miniature fiber-optic Sensor Based on Si Microresonator for Absolute Temperature Measurements. *Sens. Actuators A Phys.* **2020**, *316*, 112385. [[CrossRef](#)]
22. Pissadakis, S. Lab-in-a-fiber sensors: A review. *Microelectron. Eng.* **2019**, *217*. [[CrossRef](#)]
23. Wang, W.; Liu, T.; Yi, D. Detection of Mercury Ion Based on Quantum Dots Using Miniaturised Optical Fibre Sensor. *J. Eng.* **2019**, *2019*, 8595–8598. [[CrossRef](#)]
24. Islam, S.; Bidin, N.; Riaz, S.; Krishnan, G.; Naseem, S. Sol-gel Based Fiber Optic pH Nanosensor: Structural and Sensing Properties. *Sens. Actuators A Phys.* **2015**, *238*, 8–18. [[CrossRef](#)]
25. Ricciardi, A.; Consales, M.; Pisco, M.; Cusano, A. Application of Nanotechnology to Optical Fibre Sensors: Recent Advancements and New Trends. *Opt. Fibre Sens. Fundam. Dev. Optim. Devices* **2020**, 289–329. [[CrossRef](#)]
26. Elosua, C.; Arregui, F.J.; Del Villar, I.; Ruiz-Zamarreño, C.; Corres, J.M.; Barriain, C.; Goicoechea, J.; Hernaez, M.; Rivero, P.J.; Socorro, A.B.; et al. Micro and Nanostructured Materials for the Development of Optical Fibre Sensors. *Sensors* **2017**, *17*, 2312. [[CrossRef](#)]
27. Lu, F.; Wright, R.; Lu, P.; Cvetic, P.C.; Ohodnicki, P.R. Distributed Fiber Optic pH Sensors Using sol-gel Silica Based Sensitive Materials. *Sens. Actuators B Chem.* **2021**, *340*, 129853. [[CrossRef](#)]
28. Figueira, R.B. Hybrid Sol-Gel Coatings for Corrosion Mitigation: A Critical Review. *Polymers* **2020**, *12*, 689. [[CrossRef](#)]
29. Chu, C.-S.; Chuang, C.-Y. Optical Fiber Sensor for Dual Sensing of Dissolved Oxygen and Cu²⁺ Ions Based on PdTFPP/CdSe Embedded in sol-gel Matrix. *Sens. Actuators B Chem.* **2015**, *209*, 94–99. [[CrossRef](#)]
30. Ruan, S.; Ebendorff-Heidepriem, H.; Ruan, Y. Optical Fibre turn-on Sensor for the Detection of Mercury Based on Immobilized Fluorophore. *Measurement* **2018**, *121*, 122–126. [[CrossRef](#)]
31. Wang, H.; Liu, B.; Ding, Z.; Wang, X. Determination of Water PH Using Absorption-based Optical Sensors: Evaluation of Different Calculation Methods. In Proceedings of the International Conference on Optical and Photonics Engineering (icOPEN 2016), Chengdu, China, 26–30 September 2016; 10250, p. 102502D.
32. Inerra, B.; Hayashi, K.; Marchisio, A.; Tulliani, J.-M. Sol-gel-entrapped pH Indicator for Monitoring pH Variations in Cementitious Materials. *J. Appl. Biomater. Funct. Mater.* **2020**, *18*, 1–12. [[CrossRef](#)] [[PubMed](#)]
33. Wang, X.-D.; Wolfbeis, O.S. Fiber-Optic Chemical Sensors and Biosensors (2015–2019). *Anal. Chem.* **2019**, *92*, 397–430. [[CrossRef](#)] [[PubMed](#)]
34. Jerónimo, P.C.; Araújo, A.N.; Montenegro, M. Optical Sensors and Biosensors Based on sol-gel Films. *Talanta* **2007**, *72*, 13–27. [[CrossRef](#)]
35. Sousa, R.P.C.L.; Figueira, R.B.; Gomes, B.R.; Costa, S.P.G.; Azenha, M.; Pereira, R.F.P.; Raposo, M.M. Organic-Inorganic Hybrid sol-gel Materials Doped with a Fluorescent Triarylimidazole Derivative. *RSC Adv.* **2021**, *11*, 24613–24623. [[CrossRef](#)]
36. Chen, K.; Chou, W.; Liu, L.; Cui, Y.; Xue, P.; Jia, M. Electrochemical Sensors Fabricated by Electrospinning Technology: An Overview. *Sensors* **2019**, *19*, 3676. [[CrossRef](#)] [[PubMed](#)]
37. Ricciardi, A.; Crescitelli, A.; Vaiano, P.; Quero, G.; Consales, M.; Pisco, M.; Esposito, E.; Cusano, A. Lab-on-fiber Technology: A New Vision for Chemical and Biological Sensing. *Analyst* **2015**, *140*, 8068–8079. [[CrossRef](#)]
38. Álvarez-Botero, G.; Barón, F.; Cano, C.C.; Sosa, O.; Varon, M. Optical Sensing Using Fiber Bragg Gratings: Fundamentals and Applications. *IEEE Instrum. Meas. Mag.* **2017**, *20*, 33–38. [[CrossRef](#)]
39. Ye, X.W.; Su, Y.H.; Han, J.P. Structural Health Monitoring of Civil Infrastructure Using Optical Fiber Sensing Technology: A Comprehensive Review. *Sci. World J.* **2014**, *2014*, 1–11. [[CrossRef](#)]
40. Kousiatza, C.; Tzetzis, D.; Karalekas, D. In-situ Characterization of 3D Printed Continuous Fiber Reinforced Composites: A Methodological Study Using Fiber Bragg Grating Sensors. *Compos. Sci. Technol.* **2019**, *174*, 134–141. [[CrossRef](#)]
41. Webb, D.J. Fibre Bragg Grating Sensors in Polymer Optical Fibres. *Meas. Sci. Technol.* **2015**, *26*, 092004. [[CrossRef](#)]

42. Majumder, M.; Gangopadhyay, T.K.; Chakraborty, A.K.; Dasgupta, K.; Bhattacharya, D. Fibre Bragg Gratings in Structural Health Monitoring—Present Status and Applications. *Sens. Actuators A Phys.* **2008**, *147*, 150–164. [[CrossRef](#)]
43. Maaskant, R.; Alavie, T.; Measures, R.; Tadros, G.; Rizkalla, S.; Guha-Thakurta, A. Fiber-optic Bragg Grating Sensors for Bridge Monitoring. *Cem. Concr. Compos.* **1997**, *19*, 21–33. [[CrossRef](#)]
44. Mihailov, S.J. Fiber Bragg Grating Sensors for Harsh Environments. *Sensors* **2012**, *12*, 1898–1918. [[CrossRef](#)]
45. Li, W.; Ho, S.C.M.; Song, G. Corrosion Detection of Steel Reinforced Concrete Using Combined Carbon Fiber and Fiber Bragg Grating Active Thermal Probe. *Smart Mater. Struct.* **2016**, *25*, 045017. [[CrossRef](#)]
46. Antunes, P.; Lima, H.; Alberto, N.; Bilro, L.; Pinto, P.; Costa, A.; Rodrigues, H.; Pinto, J.L.; Nogueira, R.; Varum, H.; et al. Optical Sensors Based on Fiber Bragg Gratings for Structural Health Monitoring. In *New Developments in Sensing Technology for Structural Health Monitoring*; Lecture Notes in Electrical Engineering; Mukhopadhyay, S.C., Ed.; Springer: Heidelberg/Berlin, Germany, 2011; pp. 253–295. ISBN 978-3-642-21099-0.
47. Bremer, K.; Wollweber, M.; Weigand, F.; Rahlves, M.; Kuhne, M.; Helbig, R.; Roth, B. Fibre Optic Sensors for the Structural Health Monitoring of Building Structures. *Procedia Technol.* **2016**, *26*, 524–529. [[CrossRef](#)]
48. Sousa, R.P.C.L.; Figueira, R.B.; Costa, S.P.G.; Raposo, M.M.M. Optical Fiber Sensors for Biocide Monitoring: Examples, Transduction Materials, and Prospects. *ACS Sens.* **2020**, *5*, 3678–3709. [[CrossRef](#)] [[PubMed](#)]
49. Figueira, R.B. Electrochemical Sensors for Monitoring the Corrosion Conditions of Reinforced Concrete Structures: A Review. *Appl. Sci.* **2017**, *7*, 1157. [[CrossRef](#)]
50. Figueira, R.B.; Silva, C.J.R. Organic-Inorganic Hybrid Sol-Gel Materials for Optical Fiber Sensing Application. *Meet. Abstr.* **2020**, MA2020-02, 3369. [[CrossRef](#)]
51. Barczak, M.; McDonagh, C.; Wencel, D. Micro- and Nanostructured Sol-Gel-Based Materials for Optical Chemical Sensing (2005–2015). *Microchim. Acta* **2016**, *183*, 2085–2109. [[CrossRef](#)]
52. Tang, Z.; Gomez, D.; He, C.; Korposh, S.; Morgan, S.P.; Correia, R.; Hayes-Gill, B.; Setchfield, K.; Liu, L. A U-Shape Fibre-Optic pH Sensor Based on Hydrogen Bonding of Ethyl cellulose with a Sol-Gel matrix. *J. Lightwave Technol.* **2020**, *39*, 1557–1564. [[CrossRef](#)]
53. Yang, D.; Liu, Y.; Wang, Y.; Zhang, T.; Shao, M.; Yu, D.; Fu, H.; Jia, Z. Integrated Optic-Fiber Sensor Based on Enclosed EFPI and Structural Phase-Shift for Discriminating Measurement of Temperature, Pressure and RI. *Opt. Laser Technol.* **2020**, *126*, 106112. [[CrossRef](#)]
54. Yang, Y.; Averardi, A.; Gupta, N. An Intensity Modulation Based Fiber-Optic Loop Sensor for High Sensitivity Temperature Measurement. *Sens. Actuators A Phys.* **2019**, *297*. [[CrossRef](#)]
55. Kaya, M.; Esentürk, O. Study of Strain Measurement by Fiber Optic Sensors with a Sensitive Fiber Loop Ringdown Spectrometer. *Opt. Fiber Technol.* **2019**, *54*, 102070. [[CrossRef](#)]
56. Mahendran, R.; Wang, L.; Machavaram, V.; Pandita, S.; Chen, R.; Kukureka, S.; Fernando, G. Fiber-Optic Sensor Design for Chemical Process and Environmental Monitoring. *Opt. Lasers Eng.* **2009**, *47*, 1069–1076. [[CrossRef](#)]
57. Kim, H.J.; Shin, H.Y.; Pyeon, C.H.; Kim, S.; Lee, B. Fiber-Optic Humidity Sensor System for the Monitoring and Detection of Coolant Leakage in Nuclear Power Plants. *Nucl. Eng. Technol.* **2020**, *52*, 1689–1696. [[CrossRef](#)]
58. Chauhan, M.; Singh, V.K. Fiber Optic pH Sensor Using TiO₂-SiO₂ Composite Layer with a Temperature Cross-sensitivity Feature. *Optik* **2020**, *212*, 164709. [[CrossRef](#)]
59. Sabri, N.; Aljunid, S.A.; Salim, M.S.; Fouad, S. Fiber Optic Sensors: Short Review and Applications. In *Recent Trends in Physics of Material Science and Technology*; Gaol, F.L., Shrivastava, K., Akhtar, J., Eds.; Springer Series in Materials Science Springer: Singapore, 2015; pp. 299–311. ISBN 978-981-287-128-2.
60. Wang, X.; Shi, W.; Yun, H.; Grist, S.; Jaeger, N.A.F.; Chrostowski, L. Narrow-band Waveguide Bragg Gratings on SOI Wafers with CMOS-compatible Fabrication Process. *Opt. Express* **2012**, *20*, 15547–15558. [[CrossRef](#)]
61. Merzbacher, C.I.; Kersey, A.D.; Friebele, E.J. Fiber Optic Sensors in Concrete Structures: A Review. *Smart Mater. Struct.* **1996**, *5*, 196–208. [[CrossRef](#)]
62. Yeo, T.; Sun, T.; Grattan, K. Fibre-Optic Sensor Technologies for Humidity and Moisture Measurement. *Sens. Actuators A Phys.* **2008**, *144*, 280–295. [[CrossRef](#)]
63. Grahn, W.; Makedonski, P.; Wichern, J.; Kowalsky, W.; Wiese, S. Fiber Optic Sensors for an In-Situ Monitoring of Moisture and PH Value in Reinforced Concrete. In *Proceedings of the Imaging Spectrometry VII*; International Society for Optics and Photonics: Washington, DC, USA, 2002; Volume 4480, pp. 395–404.
64. Górriz, B.T.; Payá-Zaforteza, I.; García, P.C.; Maicas, S.S. New Fiber Optic Sensor for Monitoring Temperatures in Concrete Structures during Fires. *Sens. Actuators A Phys.* **2017**, *254*, 116–125. [[CrossRef](#)]
65. Zolkapli, M.; Saharudin, S.; Herman, S.H.; Abdullah, W.F.H. Quasi-distributed Sol-Gel Coated Fiber Optic Oxygen Sensing Probe. *Opt. Fiber Technol.* **2018**, *41*, 109–117. [[CrossRef](#)]
66. Bhardwaj, V.; Pathak, A.K.; Singh, V.K. No-core Fiber-based Highly Sensitive Optical Fiber pH Sensor. *J. Biomed. Opt.* **2017**, *22*, 057001. [[CrossRef](#)]
67. Pathak, A.K.; Singh, V.K. Fabrication and Characterization of Down-tapered Optical Fiber pH Sensor Using Sol-Gel Method. *Optik* **2017**, *149*, 288–294. [[CrossRef](#)]
68. Liu, D.; Han, W.; Mallik, A.K.; Yuan, J.; Yu, C.; Farrell, G.; Semenova, Y.; Wu, Q. High Sensitivity Sol-Gel Silica Coated Optical Fiber Sensor for Detection of Ammonia in Water. *Opt. Express* **2016**, *24*, 24179. [[CrossRef](#)]

69. Kant, R.; Tabassum, R.; Gupta, B.D. Integrating Nanohybrid Membranes of Reduced Graphene Oxide: Chitosan: Silica Sol Gel with Fiber Optic SPR for Caffeine Detection. *Nanotechnology* **2017**, *28*, 195502. [[CrossRef](#)] [[PubMed](#)]
70. Villalba, S.; Casas, J. Application of Optical Fiber Distributed Sensing to Health Monitoring of Concrete Structures. *Mech. Syst. Signal Process.* **2012**, *39*, 441–451. [[CrossRef](#)]
71. Bado, M.; Casas, J. A review of Recent Distributed Optical Fiber Sensors Applications for Civil Engineering Structural Health Monitoring. *Sensors* **2021**, *21*, 1818. [[CrossRef](#)] [[PubMed](#)]
72. Taheri, S. A Review on Five Key Sensors for Monitoring of Concrete Structures. *Constr. Build. Mater.* **2019**, *204*, 492–509. [[CrossRef](#)]
73. Wu, T.; Liu, G.; Fu, S.; Xing, F. Recent Progress of Fiber-Optic Sensors for the Structural Health Monitoring of civil Infrastructure. *Sensors* **2020**, *20*, 4517. [[CrossRef](#)] [[PubMed](#)]
74. Qing, X.P.; Chan, H.-L.; Beard, S.J.; Ooi, T.K.; Marotta, S.A. Effect of Adhesive on the Performance of Piezoelectric Elements used to Monitor Structural Health. *Int. J. Adhes. Adhes.* **2006**, *26*, 622–628. [[CrossRef](#)]
75. Liu, W.; Giurgiutiu, V. Finite Element Simulation of Piezoelectric Wafer Active Sensors for Structural Health Monitoring with Coupled-filed Elements. *Proc. SPIE* **2007**, 6529, 65293. [[CrossRef](#)]
76. Li, X.; Cui, H.; Zhang, B.; Yuan, C. Experimental Study of a Structural Health Monitoring Method Based on Piezoelectric Element Array. In Proceedings of the 2017 IEEE 3rd Information Technology and Mechatronics Engineering Conference (ITOEC), Chongqing, China, 3–5 October 2017; pp. 27–31.
77. Nie, M.; Xia, Y.-H.; Yang, H.-S. A Flexible and Highly Sensitive Graphene-Based Strain Sensor for Structural Health Monitoring. *Clust. Comput.* **2018**, *22*, 8217–8224. [[CrossRef](#)]
78. Li, X.D.; Li, S.L.; Zhong, S.L.; Ge, S. Comparison Analysis of Fiber Bragg Brating and Resistance Strain Gauge Used in Quayside Container Crane Structural Health Monitoring. *Appl. Mech. Mater.* **2013**, *330*, 485–493. [[CrossRef](#)]
79. Leung, C.K.Y.; Wan, K.T.; Inaudi, D.; Bao, X.; Habel, W.; Zhou, Z.; Ou, J.; Ghandehari, M.; Wu, H.C.; Imai, M. Review: Optical Fiber Sensors for Civil Engineering Applications. *Mater. Struct.* **2013**, *48*, 871–906. [[CrossRef](#)]
80. Rajeev, P.; Kodikara, J.; Chiu, W.K.; Kuen, T. Distributed Optical Fibre Sensors and Their Applications in Pipeline Monitoring. *Key Eng. Mater.* **2013**, *558*, 424–434. [[CrossRef](#)]
81. Takeda, S.-I.; Aoki, Y.; Nagao, Y. Damage Monitoring of CFRP Stiffened Panels Under Compressive Load Using FBG Sensors. *Compos. Struct.* **2012**, *94*, 813–819. [[CrossRef](#)]
82. Tan, C.; Shee, Y.G.; Yap, B.; Adikan, F.M. Fiber Bragg Grating Based Sensing System: Early Corrosion Detection for Structural Health Monitoring. *Sens. Actuators A Phys.* **2016**, *246*, 123–128. [[CrossRef](#)]
83. Yehia, S.; Landolsi, T.; Hassan, M.; Hallal, M. Monitoring of Strain Induced by Heat of Hydration, Cyclic and Dynamic Loads in Concrete Structures Using Fiber-Optics Sensors. *Measurement* **2014**, *52*, 33–46. [[CrossRef](#)]
84. Royon, M.; Jamon, D.; Blanchet, T.; Royer, F.; Vocanson, F.; Marin, E.; Morana, A.; Boukenter, A.; Ouerdane, Y.; Jourlin, Y.; et al. Sol–Gel Waveguide-Based Sensor for Structural Health Monitoring on Large Surfaces in Aerospace Domain. *Aerospace* **2021**, *8*, 109. [[CrossRef](#)]
85. Silva, R.N.F.; Tsuruta, K.M.; Rabelo, D.S.; Neto, R.M.F.; Cavalini, A.A.; Steffen, V. Impedance-Based Structural Health Monitoring Applied to Steel Fiber-Reinforced Concrete Structures. *J. Braz. Soc. Mech. Sci. Eng.* **2020**, *42*, 1–15. [[CrossRef](#)]
86. Sakiyama, F.I.H.; Lehmann, F.; Garrecht, H. Structural Health Monitoring of Concrete Structures Using Fibre-Optic-Based Sensors: A Review. *Mag. Concr. Res.* **2021**, *73*, 174–194. [[CrossRef](#)]
87. Rossi, P.; Le Maou, F. New Method for Detecting Cracks in Concrete Using Fibre Optics. *Mater. Struct.* **1989**, *22*, 437–442. [[CrossRef](#)]
88. Bao, T.; Wang, J.; Yao, Y. A Fiber Optic Sensor for Detecting and Monitoring Cracks in Concrete Structures. *Sci. China Ser. E Technol. Sci.* **2010**, *53*, 3045–3050. [[CrossRef](#)]
89. Deng, L.; Cai, C. Applications of Fiber Optic Sensors in Civil Engineering. *Struct. Eng. Mech.* **2007**, *25*, 577–596. [[CrossRef](#)]
90. Gerlach, G.; Guenther, M.; Suchanek, G.; Sorber, J.; Arndt, K.-F.; Richter, A. Application of Sensitive Hydrogels in Chemical and pH Sensors. *Macromol. Symp.* **2004**, *210*, 403–410. [[CrossRef](#)]
91. Manjakkal, L.; Cvejin, K.; Kulawik, J.; Zaraska, K.; Szwagierczak, D.; Stojanovic, G. Sensing Mechanism of RuO₂–SnO₂ Thick Film pH Sensors Studied by Potentiometric Method and Electrochemical Impedance Spectroscopy. *J. Electroanal. Chem.* **2015**, *759*, 82–90. [[CrossRef](#)]
92. Ke, X. Micro-fabricated Electrochemical Chloride Ion Sensors: From the Present to the Future. *Talanta* **2020**, *211*, 120734. [[CrossRef](#)] [[PubMed](#)]
93. Manjakkal, L.; Szwagierczak, D.; Dahiya, R. Metal Oxides Based Electrochemical pH Sensors: Current Progress and Future Perspectives. *Prog. Mater. Sci.* **2019**, *109*, 100635. [[CrossRef](#)]
94. Huang, W.-D.; Cao, H.; Deb, S.; Chiao, M.; Chiao, J. A Flexible pH Sensor Based on the Iridium Oxide Sensing Film. *Sens. Actuators A Phys.* **2011**, *169*, 1–11. [[CrossRef](#)]
95. Grant, S.A.; Bettencourt, K.; Krulevitch, P.; Hamilton, J.; Glass, R. In Vitro and in Vivo Measurements of Fiber Optic and Electrochemical Sensors to Monitor Brain Tissue pH. *Sens. Actuators B Chem.* **2001**, *72*, 174–179. [[CrossRef](#)]
96. O'Hare, D.; Parker, K.H.; Winlove, C.P. Metal–Metal Oxide pH Sensors for Physiological Application. *Med. Eng. Phys.* **2006**, *28*, 982–988. [[CrossRef](#)]
97. Alam, A.U.; Qin, Y.; Nambiar, S.; Yeow, J.T.; Howlader, M.M.; Hu, N.-X.; Deen, J. Polymers and Organic Materials-based pH Sensors for Healthcare Applications. *Prog. Mater. Sci.* **2018**, *96*, 174–216. [[CrossRef](#)]

98. Nguyen, C.M.; Rao, S.; Yang, X.; Dubey, S.; Mays, J.; Cao, H.; Chiao, J.-C. Sol-gel Deposition of Iridium Oxide for Biomedical Micro-devices. *Sensors* **2015**, *15*, 4212–4228. [[CrossRef](#)]
99. Vasylevska, A.S.; Karasyov, A.A.; Borisov, S.; Krause, C. Novel Coumarin-based Fluorescent pH Indicators, Probes and Membranes Covering a Broad pH Range. *Anal. Bioanal. Chem.* **2007**, *387*, 2131–2141. [[CrossRef](#)] [[PubMed](#)]
100. Wolfbeis, O.S. Fiber-Optic Chemical Sensors and Biosensors. *Anal. Chem.* **2008**, *80*, 4269–4283. [[CrossRef](#)] [[PubMed](#)]
101. Kim, T.Y.; Yang, S. Fabrication method and characterization of electrodeposited and heat-treated iridium oxide films for pH sensing. *Sens. Actuators B Chem.* **2014**, *196*, 31–38. [[CrossRef](#)]
102. Mihell, J.; Atkinson, J. Planar Thick-film pH Electrodes Based on Ruthenium Dioxide Hydrate. *Sens. Actuators B Chem.* **1998**, *48*, 505–511. [[CrossRef](#)]
103. Ryyänen, T.; Nurminen, K.; Hämäläinen, J.; Leskela, M.; Lekkala, J. pH Electrode Based on ALD Deposited Iridium Oxide. *Procedia Eng.* **2010**, *5*, 548–551. [[CrossRef](#)]
104. Manjakkal, L.; Cvejic, K.; Kulawik, J.; Zaraska, K.; Szwagierczak, D.; Socha, R.P. Fabrication of Thick Film Sensitive RuO₂-TiO₂ and Ag/AgCl/KCl Reference Electrodes and Their Application for pH Measurements. *Sens. Actuators B Chem.* **2014**, *204*, 57–67. [[CrossRef](#)]
105. Liu, B.; Zhang, J. A Ruthenium Oxide and Iridium Oxide Coated Titanium Electrode for pH Measurement. *RSC Adv.* **2020**, *10*, 25952–25957. [[CrossRef](#)]
106. Da Silva, G.; Lemos, S.; Pocrifka, L.; Marreto, P.; Rosario, A.; Pereira, E. Development of Low-cost Metal Oxide pH Electrodes Based on the Polymeric Precursor Method. *Anal. Chim. Acta* **2008**, *616*, 36–41. [[CrossRef](#)]
107. Zhou, Z.; Li, J.; Pan, D.; Wei, H.; Wang, C.; Pan, F.; Xia, J.; Ma, S. pH Electrodes Based on Iridium Oxide Films for Marine Monitoring. *Trends Environ. Anal. Chem.* **2020**, *25*, e00083. [[CrossRef](#)]
108. El-Giar, E.E.-D.M.; Wipf, D. Microparticle-based Iridium Oxide Ultramicroelectrodes for pH Sensing and Imaging. *J. Electroanal. Chem.* **2007**, *609*, 147–154. [[CrossRef](#)]
109. Sardarinejad, A.; Maurya, D.K.; Alameh, K. The pH Sensing Properties of RF Sputtered RuO₂ Thin-film Prepared Using Different Ar/O₂ Flow Ratio. *Materials* **2015**, *8*, 3352–3363. [[CrossRef](#)]
110. Shylendra, S.P.; Lonsdale, W.; Wajrak, M.; Nur-E-Alam, M.; Alameh, K. Titanium Nitride Thin Film Based Low-Redox-Interference Potentiometric pH Sensing Electrodes. *Sensors* **2020**, *21*, 42. [[CrossRef](#)] [[PubMed](#)]
111. Deibert, B.J.; Li, J. A Distinct Reversible Colorimetric and Fluorescent Low pH Response on a Water-Stable Zirconium–Porphyrin Metal–Organic Framework. *Chem. Commun.* **2014**, *50*, 9636–9639. [[CrossRef](#)] [[PubMed](#)]
112. Huang, X.-R.; Ren, Q.-Q.; Yuan, X.-J.; Wen, W.; Chen, W.; Zhan, D.-P. Iridium Oxide Based Coaxial pH Ultramicroelectrode. *Electrochem. Commun.* **2014**, *40*, 35–37. [[CrossRef](#)]
113. Koncki, R.; Mascini, M. Screen-Printed Ruthenium Dioxide Electrodes for pH Measurements. *Anal. Chim. Acta* **1997**, *351*, 143–149. [[CrossRef](#)]
114. Bause, S.; Decker, M.; Gerlach, F.; Nather, J.; Köster, F.; Neubauer, P.; Vonau, W. Development of an Iridium-based pH Sensor for Bioanalytical Applications. *J. Solid State Electrochem.* **2017**, *22*, 51–60. [[CrossRef](#)]
115. Zimer, A.M.; Lemos, S.; Pocrifka, L.; Mascaro, L.; Pereira, E. Needle-like IrO/Ag Combined pH Microelectrode. *Electrochem. Commun.* **2010**, *12*, 1703–1705. [[CrossRef](#)]
116. Sardarinejad, A.; Maurya, D.; Alameh, K. The Effects of Sensing Electrode Thickness on Ruthenium Oxide Thin-Film pH Sensor. *Sens. Actuators A Phys.* **2014**, *214*, 15–19. [[CrossRef](#)]
117. Ferreira, R.C.M.; Costa, S.P.G.; Gonçalves, H.; Belsley, M.; Raposo, M.M.M. Fluorescent Phenanthroimidazoles Functionalized with Heterocyclic Spacers: Synthesis, optical chemosensory ability and two-photon absorption (TPA) properties. *New J. Chem.* **2017**, *41*, 12866–12878. [[CrossRef](#)]
118. Esteves, C.I.; Ferreira, R.M.; Raposo, M.M.; Costa, S.P. New Fluoroionophores for Metal Cations Based on Benzo[d]oxazol-5-yl-alanine Bearing Pyrrole and Imidazole. *Dye. Pigment.* **2018**, *151*, 211–218. [[CrossRef](#)]
119. Debus, H. Ueber Die Einwirkung Des Ammoniaks Auf Glyoxal. *Eur. J. Org. Chem.* **1858**, *107*, 199–208. [[CrossRef](#)]
120. Sundberg, R.J.; Martin, R.B. Interactions of Histidine and Other Imidazole Derivatives with Transition Metal Ions in Chemical and Biological Systems. *Chem. Rev.* **1974**, *74*, 471–517. [[CrossRef](#)]
121. Graßmann, S.; Apelt, J.; Sippl, W.; Ligneau, X.; Pertz, H.H.; Zhao, Y.H.; Arrang, J.-M.; Ganellin, C.; Schwartz, J.-C.; Schunack, W.; et al. Imidazole Derivatives as a Novel Class of Hybrid Compounds with Inhibitory Histamine N-methyltransferase Potencies and Histamine h₃ Receptor Affinities. *Bioorg. Med. Chem.* **2003**, *11*, 2163–2174. [[CrossRef](#)]
122. Sharma, A.; Kumar, V.; Kharb, R.; Kumar, S.; Chander Sharma, P.; Pal Pathak, D. Imidazole Derivatives as Potential Therapeutic Agents. *Curr. Pharm. Des.* **2016**, *22*, 3265–3301. [[CrossRef](#)]
123. Molina, P.; Tárraga, A.; Otón, F. Imidazole Derivatives: A Comprehensive Survey of Their Recognition Properties. *Org. Biomol. Chem.* **2011**, *10*, 1711–1724. [[CrossRef](#)]
124. Lv, H.; Zhao, X.; Zhan, Y.; Gong, P. Damage Evaluation of Concrete Based on Brillouin Corrosion Expansion Sensor. *Constr. Build. Mater.* **2017**, *143*, 387–394. [[CrossRef](#)]
125. Abbas, Y.; ten Have, B.; Hoekstra, G.I.; Douma, A.; de Bruijn, D.; Olthuis, W.; van den Berg, A. Connecting to Concrete: Wireless Monitoring of Chloride Ions in Concrete Structures. *Procedia Eng.* **2015**, *120*, 965–968. [[CrossRef](#)]
126. Ansari, F. Fiber Optic Health Monitoring of Civil Structures Using Long Gage and Acoustic Sensors. *Smart Mater. Struct.* **2005**, *14*, S1–S7. [[CrossRef](#)]

127. Dong, S.-G.; Lin, C.-J.; Hu, R.-G.; Li, L.-Q.; Du, R.-G. Effective Monitoring of Corrosion in Reinforcing Steel in Concrete Constructions by a Multifunctional Sensor. *Electrochim. Acta* **2010**, *56*, 1881–1888. [[CrossRef](#)]
128. Bartelmess, J.; Zimmek, D.; Bartholmai, M.; Strangfeld, C.; Schäferling, M. Fibre Optic Ratiometric Fluorescence pH Sensor for Monitoring Corrosion in Concrete. *Analyst* **2020**, *145*, 2111–2117. [[CrossRef](#)] [[PubMed](#)]
129. Tariq, A.; Baydoun, J.; Remy, C.; Ghasemi, R.; Lefevre, J.P.; Mongin, C.; Dauzères, A.; Leray, I. Fluorescent Molecular Probe Based Optical Fiber Sensor Dedicated to pH Measurement of Concrete. *Sens. Actuators B Chem.* **2020**, *327*, 128906. [[CrossRef](#)]
130. Hall, S.K.; Stableforth, D.E.; Green, A. Sweat Sodium and Chloride Concentrations—Essential Criteria for the Diagnosis of Cystic Fibrosis in Adults. *Ann. Clin. Biochem. Int. J. Lab. Med.* **1990**, *27*, 318–320. [[CrossRef](#)]
131. Gonzalo-Ruiz, J.; Mas, R.; de Haro, C.; Cabruja, E.; Camero, R.; Alonso-Lomillo, M.A.; Muñoz, F.J. Early Determination of Cystic Fibrosis by Electrochemical Chloride Quantification in Sweat. *Biosens. Bioelectron.* **2009**, *24*, 1788–1791. [[CrossRef](#)] [[PubMed](#)]
132. Cuartero, M.; Parrilla, M.; Crespo, G.A. Wearable Potentiometric Sensors for Medical Applications. *Sensors* **2019**, *19*, 363. [[CrossRef](#)] [[PubMed](#)]
133. Laxmeshwar, L.S.; Jadhav, M.S.; Akki, J.F.; Raikar, P.; Kumar, J.; Prakash, O.; Mahakud, R.; Raikar, U.; Laxmeshwara, L.S. Quantification of Chloride and Iron in Sugar Factory Effluent Using Long Period Fiber Grating Chemical Sensor. *Sens. Actuators B Chem.* **2018**, *258*, 850–856. [[CrossRef](#)]
134. Asche, K.; Fontenot, S.; Lee, S. *City of Morris—Chloride Discharge Assessment*; Center for Small Towns: Morris, MN, USA, 2013; Volume 66, Available online: <https://digitalcommons.morris.umn.edu/cst/66>.
135. Bujes-Garrido, J.; Arcos-Martínez, M.J. Disposable Sensor for Electrochemical Determination of Chloride Ions. *Talanta* **2016**, *155*, 153–157. [[CrossRef](#)]
136. Guo, Y.; Compton, R.G. A Bespoke Reagent free Amperometric Chloride Sensor for Drinking Water. *Analyst* **2021**, *146*, 4700–4707. [[CrossRef](#)]
137. Atkins, C.; Carter, M.; Scantlebury, J. Sources of Error in Using Silver/Silver Chloride Electrodes to Monitor Chloride Activity in Concrete. *Cem. Concr. Res.* **2001**, *31*, 1207–1211. [[CrossRef](#)]
138. Gandña-Romero, J.M.; Bataller, R.; Monzón, P.; Campos, I.; García-Breijó, E.; Valcuende, M.; Soto, J. Characterization of Embeddable Potentiometric Thick-Film Sensors for Monitoring Chloride Penetration in Concrete. *Sens. Actuators B Chem.* **2016**, *222*, 407–418. [[CrossRef](#)]
139. Tian, Y.; Zhang, P.; Zhao, K.; Du, Z.; Zhao, T. Application of Ag/AgCl Sensor for Chloride Monitoring of Mortar Under Dry-Wet Cycles. *Sensors* **2020**, *20*, 1394. [[CrossRef](#)]
140. Abbas, Y.; Pargar, F.; Koleva, D.A.; van Breugel, K.; Olthuis, W.; Berg, A.V.D. Non-Destructive Measurement of Chloride Ions Concentration in Concrete—A Comparative Analysis of Limitations and Prospects. *Constr. Build. Mater.* **2018**, *174*, 376–387. [[CrossRef](#)]
141. Melo, L.; Rodrigues, J.; Farinha, A.; Marques, C.; Bilro, L.; Alberto, N.; Tomé, J.; Nogueira, R. Concentration Sensor Based on a Tilted Fiber Bragg Grating for Anions Monitoring. *Opt. Fiber Technol.* **2014**, *20*, 422–427. [[CrossRef](#)]
142. Tang, J.-L.; Wang, J.-N. Measurement of Chloride-Ion Concentration With Long-Period Grating Technology. *Smart Mater. Struct.* **2007**, *16*, 665–672. [[CrossRef](#)]
143. Glasser, F.P.; Marchand, J.; Samson, E. Durability of concrete—Degradation Phenomena Involving Detrimental Chemical Reactions. *Cem. Concr. Res.* **2008**, *38*, 226–246. [[CrossRef](#)]
144. Andrade, C.; Keddah, M.; Nóvoa, X.; Pérez, M.C.; Rangel, C.M.; Takenouti, H. Electrochemical Behaviour of Steel Rebars in Concrete: Influence of Environmental Factors and Cement Chemistry. *Electrochim. Acta* **2001**, *46*, 3905–3912. [[CrossRef](#)]
145. Muthulingam, S.; Rao, B.N. Chloride Binding and Time-Dependent Surface Chloride Content Models for Fly Ash Concrete. *Front. Struct. Civ. Eng.* **2015**, *10*, 112–120. [[CrossRef](#)]
146. Cady, P.; Weyers, R. Predicting Service Life of Concrete Bridge Decks Subject to Reinforcement Corrosion. *ASTM Int.* **2009**, 328. [[CrossRef](#)]
147. Darmawan, M.S. Pitting Corrosion Model for Reinforced Concrete Structures in a Chloride Environment. *Mag. Concr. Res.* **2010**, *62*, 91–101. [[CrossRef](#)]
148. Li, D.; Wei, R.; Li, L.; Guan, X.; Mi, X. Pitting Corrosion of Reinforcing Steel Bars in Chloride Contaminated Concrete. *Constr. Build. Mater.* **2018**, *199*, 359–368. [[CrossRef](#)]
149. Ann, K.Y.; Song, H.-W. Chloride Threshold Level for Corrosion of Steel in Concrete. *Corros. Sci.* **2007**, *49*, 4113–4133. [[CrossRef](#)]
150. Basheer, L.; Kropp, J.; Cleland, D.J. Assessment of the Durability of Concrete From its Permeation Properties: A Review. *Constr. Build. Mater.* **2001**, *15*, 93–103. [[CrossRef](#)]
151. Kwon, S.-J.; Lee, H.-S.; Karthick, S.; Saraswathy, V.; Yang, H.-M. Long-term Corrosion Performance of Blended Cement Concrete in the Marine Environment—A Real-time Study. *Constr. Build. Mater.* **2017**, *154*, 349–360. [[CrossRef](#)]
152. Figueira, R.M.B.B.M.; Fontinha, I.R.; Silva, C.J.R.; Pereira, E.V. Hybrid Sol-gel Coatings: Smart and Green Materials for Corrosion Mitigation. *Coatings* **2016**, *6*, 12. [[CrossRef](#)]
153. Lu, C.; Jin, W.; Liu, R. Reinforcement Corrosion-induced Cover Cracking and its Time Prediction for Reinforced Concrete Structures. *Corros. Sci.* **2011**, *53*, 1337–1347. [[CrossRef](#)]
154. Feliu, S.; González, J.; Miranda, J.M.; Feliu, V. Possibilities and Problems of in Situ Techniques for Measuring Steel Corrosion Rates in Large Reinforced Concrete Structures. *Corros. Sci.* **2005**, *47*, 217–238. [[CrossRef](#)]

155. Song, H.-W.; Lee, C.-H.; Ann, K.Y. Factors Influencing Chloride Transport in Concrete Structures Exposed to Marine Environments. *Cem. Concr. Compos.* **2008**, *30*, 113–121. [[CrossRef](#)]
156. Hong, K.; Hooton, R.D. Effects of Cyclic Chloride Exposure on Penetration of Concrete Cover. *Cem. Concr. Res.* **1999**, *29*, 1379–1386. [[CrossRef](#)]
157. Shi, X.; Xie, N.; Fortune, K.; Gong, J. Durability of Steel Reinforced Concrete in Chloride Environments: An Overview. *Constr. Build. Mater.* **2012**, *30*, 125–138. [[CrossRef](#)]
158. Hansson, C.M. The Impact of Corrosion on Society. *Met. Mater. Trans. A* **2011**, *42*, 2952–2962. [[CrossRef](#)]
159. Dodds, W.; Christodoulou, C.; Goodier, C.; Austin, S.; Dunne, D. Durability Performance of Sustainable Structural Concrete: Effect of Coarse Crushed Concrete Aggregate on Rapid Chloride Migration and Accelerated Corrosion. *Constr. Build. Mater.* **2017**, *155*, 511–521. [[CrossRef](#)]
160. Chen, E.; Berrocal, C.G.; Löfgren, I.; Lundgren, K. Correlation Between Concrete Cracks and Corrosion Characteristics of Steel Reinforcement in Pre-cracked Plain and Fibre-Reinforced Concrete Beams. *Mater. Struct.* **2020**, *53*, 1–22. [[CrossRef](#)]
161. Yu, H.; Chiang, K.-T.K.; Yang, L. Threshold Chloride Level and Characteristics of Reinforcement Corrosion Initiation in Simulated Concrete Pore Solutions. *Constr. Build. Mater.* **2012**, *26*, 723–729. [[CrossRef](#)]
162. Luo, D.; Ma, J.; Ibrahim, Z.; Ismail, Z. Etched FBG Coated with Polyimide for Simultaneous Detection the Salinity and Temperature. *Opt. Commun.* **2017**, *392*, 218–222. [[CrossRef](#)]
163. Ding, L.; Li, Z.; Ding, Q.; Shen, X.; Yuan, Y.; Huang, J. Microstructured Optical Fiber Based Chloride Ion Sensing Method for Concrete Health Monitoring. *Sens. Actuators B Chem.* **2018**, *260*, 763–769. [[CrossRef](#)]
164. Dhoub, M.; Conciatori, D.; Sorelli, L. Optical Fiber Chloride Sensor for Health Monitoring of Structures in Cold Regions. In *Cold Regions Engineering*; Reston, V.A., Ed.; American Society of Civil Engineers: Reston, VI, USA, 2019; pp. 391–397. [[CrossRef](#)]
165. Xiao, W.; Ding, L.; He, J.; Huang, J. Preparation of Lucigenin-Doped Silica Nanoparticles and Their Application in Fiber Optic Chloride Ion Sensor. *Opt. Mater.* **2019**, *98*, 109467. [[CrossRef](#)]
166. Tang, F.; Li, Z.; Li, C.; Chen, Y.; Li, H.-N. Monitoring Passivation, Pitting Corrosion Initiation, and Propagation of Steel Bar with Iron–Carbon Electroplated Long Period Fiber–Grating Sensor. *J. Mater. Civ. Eng.* **2020**, *32*, 04020373. [[CrossRef](#)]
167. Valero, L.R.; Sasso, V.F.; Vicioso, E.P. In Situ Assessment of Superficial Moisture Condition in Façades of Historic Building Using Non-Destructive Techniques. *Case Stud. Constr. Mater.* **2019**, *10*, e00228. [[CrossRef](#)]
168. Zhou, W.; Xu, Z.; Ross, D.; Dignan, J.; Fan, Y.; Huang, Y.; Wang, G.; Bagtzoglou, A.C.; Lei, Y.; Li, B. Towards Water-Saving Irrigation Methodology: Field Test of Soil Moisture Profiling Using Flat Thin mm-sized Soil Moisture Sensors (MSMSs). *Sens. Actuators B Chem.* **2019**, *298*, 126857. [[CrossRef](#)]
169. Zheng, L.R.; Tenhunen, H.; Zou, Z. Intelligent Packaging: Humidity Sensing System. In *Smart Electronic Systems*; John Wiley & Sons, Ltd: Hoboken, NJ, USA, 2018; pp. 205–220. ISBN 978-3-527-69168-5.
170. Dean, T.; Bell, J.; Baty, A. Soil Moisture Measurement by an Improved Capacitance Technique, Part I. Sensor Design and Performance. *J. Hydrol.* **1987**, *93*, 67–78. [[CrossRef](#)]
171. Kizito, F.; Campbell, C.S.; Campbell, G.S.; Cobos, D.R.; Teare, B.L.; Carter, B.; Hopmans, J.W. Frequency, Electrical Conductivity and Temperature Analysis of a Low-Cost Capacitance Soil Moisture Sensor. *J. Hydrol.* **2008**, *352*, 367–378. [[CrossRef](#)]
172. Voss, A.; Pour-Ghaz, M.; Vauhkonen, M.; Seppänen, A. Electrical Capacitance Tomography to Monitor Unsaturated Moisture Ingress In Cement-Based Materials. *Cem. Concr. Res.* **2016**, *89*, 158–167. [[CrossRef](#)]
173. Kim, H.-S.; Kim, J.H.; Park, S.-Y.; Kang, J.-H.; Kim, S.-J.; Choi, Y.-B.; Shin, U.S. Carbon Nanotubes Immobilized on Gold Electrode As an Electrochemical Humidity Sensor. *Sens. Actuators B Chem.* **2019**, *300*, 127049. [[CrossRef](#)]
174. Qi, R.; Lin, X.; Dai, J.; Zhao, H.; Liu, S.; Fei, T.; Zhang, T. Humidity Sensors Based on MCM-41/Polypyrrole Hybrid Film Via In-Situ Polymerization. *Sens. Actuators B Chem.* **2018**, *277*, 584–590. [[CrossRef](#)]
175. Alwis, L.; Sun, T.; Grattan, K. Optical Fibre-Based Sensor Technology for Humidity and Moisture Measurement: Review of Recent Progress. *Measurement* **2013**, *46*, 4052–4074. [[CrossRef](#)]
176. Paroll, H.; Nykänen, E. Measurement of Relative Humidity and Temperature in a New Concrete Bridge vs Laboratory Samples. In *Proceedings of the Nordic Concrete Research*; Norsk Betongforening: Oslo, Norway, 1999; Volume 23, pp. 116–118.
177. Shoukry, S.N.; William, G.W.; Downie, B.; Riad, M.Y. Effect of Moisture and Temperature on the Mechanical Properties of Concrete. *Constr. Build. Mater.* **2011**, *25*, 688–696. [[CrossRef](#)]
178. Kim, J.-K.; Lee, C.-S. Moisture Diffusion of Concrete Considering Self-Desiccation at Early Ages. *Cem. Concr. Res.* **1999**, *29*, 1921–1927. [[CrossRef](#)]
179. Neville, A.M. *Properties of Concrete: Fourth and Final Edition*; Wiley: Hoboken, NJ, USA, 1996; ISBN 978-0-470-23527-0.
180. Straube, J. Moisture in Buildings. *ASHRAE J.* **2002**, *44*, 15–19.
181. Nemeč, T.; Rant, J.; Apih, V.; Kaling, M. Monitoring of Moisture Transport in Building Materials by Neutron Radiography. In *Proceedings of the 7th European Conference on Non-Destructive Testing*, Copenhagen, Denmark, 26–29 May 1998; pp. 822–828, ISBN 978-87-986898-0-5.
182. Norris, A.; Saafi, M.; Romine, P. Temperature and Moisture Monitoring in Concrete Structures Using Embedded Nanotechnology/Microelectromechanical Systems (MEMS) Sensors. *Constr. Build. Mater.* **2008**, *22*, 111–120. [[CrossRef](#)]
183. Dong, Y.; Luke, A.; Vitillo, N.; Ansari, F. In-place Estimation of Concrete Strength During the Construction of a Highway Bridge By the Maturity Method. *Concr. Int.* **2002**, *24*, 61–66.

184. Harith, Z.; Batumalay, M.; Irawati, N.; Harun, S.; Arof, H.; Ahmad, H. Relative Humidity Sensor Employing Tapered Plastic Optical Fiber Coated with Seeded Al-doped ZnO. *Optik* **2017**, *144*, 257–262. [[CrossRef](#)]
185. Lee, C.-Y.; Lee, G.-B. Humidity Sensors: A Review. *Sens. Lett.* **2005**, *3*, 1–15. [[CrossRef](#)]
186. Cao, D.; Fang, H.; Wang, F.; Zhu, H.; Sun, M. A Fiber Bragg-Grating-Based Miniature Sensor for the Fast Detection of Soil Moisture Profiles in Highway Slopes and Subgrades. *Sensors* **2018**, *18*, 4431. [[CrossRef](#)] [[PubMed](#)]
187. Yan, K.; Liu, J.; Sun, N.; Zhong, W. Soil Moisture Sensor Design Based on Fiber Bragg Grating. In Proceedings of the Tenth International Symposium on Precision Engineering Measurements and Instrumentation, Kunming, China, 8–10 August 2018; 2019; p. 75.
188. Islam, R.; Ali, M.M.; Lai, M.-H.; Lim, K.-S.; Ahmad, H. Chronology of Fabry-Perot Interferometer Fiber-Optic Sensors and Their Applications: A Review. *Sensors* **2014**, *14*, 7451–7488. [[CrossRef](#)]
189. Shi, J.; Xu, D.; Xu, W.; Wang, Y.; Yan, C.; Zhang, C.; Yan, D.; He, Y.; Tang, L.; Zhang, W.; et al. Humidity Sensor Based on Fabry-Perot Interferometer and Intracavity Sensing of Fiber Laser. *J. Lightwave Technol.* **2017**, *35*, 4789–4795. [[CrossRef](#)]
190. Shrivastav, A.M.; Gunawardena, D.S.; Liu, Z.; Tam, H.-Y. Microstructured Optical Fiber Based Fabry-Pérot Interferometer As a Humidity Sensor Utilizing Chitosan Polymeric Matrix for Breath Monitoring. *Sci. Rep.* **2020**, *10*, 1–10. [[CrossRef](#)] [[PubMed](#)]
191. Johari, A.M.; Khudus, M.I.M.A.; Bin Jali, M.H.; Al Noman, A.; Harun, S.W. Whispering Gallery Modes on Optical Micro-Bottle Resonator for Humidity Sensor Application. *Optik* **2019**, *185*, 558–565. [[CrossRef](#)]
192. Liang, L.; Li, M.; Liu, N.; Sun, H.; Rong, Q.; Hu, M. A High-Sensitivity Optical Fiber Relative Humidity Sensor Based on Microsphere WGM Resonator. *Opt. Fiber Technol.* **2018**, *45*, 415–418. [[CrossRef](#)]
193. Manju, P.; Hardman, K.S.; Wigley, P.B.; Close, J.D.; Robins, N.P.; Szigeti, S.S. An Atomic Fabry-Perot Interferometer Using a Pulsed Interacting Bose-Einstein Condensate. *Sci. Rep.* **2020**, *10*, 1–11. [[CrossRef](#)] [[PubMed](#)]
194. Lux, O.; Sarang, S.; Kitzler, O.; Spence, D.J.; Mildren, R.P. Intrinsically Stable High-Power Single Longitudinal Mode Laser Using Spatial Hole Burning Free Gain. *Optica* **2016**, *3*, 876–881. [[CrossRef](#)]
195. Wang, Y.-C.; Shyu, L.-H.; Chang, C.-P. The Comparison of Environmental Effects on Michelson and Fabry-Perot Interferometers Utilized for the Displacement Measurement. *Sensors* **2010**, *10*, 2577–2586. [[CrossRef](#)]
196. Foreman, M.; Swaim, J.D.; Vollmer, F. Whispering Gallery Mode Sensors. *Adv. Opt. Photon.* **2015**, *7*, 168–240. [[CrossRef](#)] [[PubMed](#)]
197. Yeo, T.L.; Eckstein, D.; McKinley, B.; Boswell, L.F.; Sun, T.; Grattan, K.T.V. Demonstration of a Fibre-Optic Sensing Technique for the Measurement of Moisture Absorption in Concrete. *Smart Mater. Struct.* **2006**, *15*, N40–N45. [[CrossRef](#)]
198. Yuan, D.; Dong, Y.; Liu, Y.; Li, T. Mach-Zehnder Interferometer Biochemical Sensor Based on Silicon-on-Insulator Rib WaveGuide with Large Cross Section. *Sensors* **2015**, *15*, 21500–21517. [[CrossRef](#)] [[PubMed](#)]
199. Zisis, G.; Ying, C.Y.J.; Soergel, E.; Mailis, S. Ferroelectric Domain Building Blocks for Photonic and Nonlinear Optical Microstructures in LiNbO₃. *J. Appl. Phys.* **2014**, *115*, 124102. [[CrossRef](#)]
200. Zhang, S.; Dong, X.; Li, T.; Chan, C.C.; Shum, P.P. Simultaneous Measurement of Relative Humidity and Temperature with PCF-MZI Cascaded by Fiber Bragg Grating. *Opt. Commun.* **2013**, *303*, 42–45. [[CrossRef](#)]
201. Yeo, T.; Sun, T.; Grattan, K.; Parry, D.; Lade, R.; Powell, B. Polymer-Coated Fiber Bragg Grating for Relative Humidity Sensing. *IEEE Sens. J.* **2005**, *5*, 1082–1089. [[CrossRef](#)]
202. Wang, Y.; Shen, C.; Lou, W.; Shentu, F. Polarization-Dependent Humidity Sensor Based on an In-Fiber Mach-Zehnder Interferometer Coated with Graphene Oxide. *Sens. Actuators B Chem.* **2016**, *234*, 503–509. [[CrossRef](#)]
203. Bian, C.; Cheng, Y.; Zhu, W.; Tong, R.; Hu, M.; Gang, T. A Novel Optical Fiber Mach-Zehnder Interferometer Based on the Calcium Alginate Hydrogel Film for Humidity Sensing. *IEEE Sens. J.* **2020**, *20*, 5759–5765. [[CrossRef](#)]
204. Blank, T.; Eksperiandova, L.; Belikov, K. Recent Trends of Ceramic Humidity Sensors Development: A Review. *Sens. Actuators B Chem.* **2016**, *228*, 416–442. [[CrossRef](#)]
205. Vipulanandan, C.; Amani, N. Characterizing the Pulse Velocity and Electrical Resistivity Changes in Concrete with Piezoresistive Smart Cement Binder Using Vipulanandan Models. *Constr. Build. Mater.* **2018**, *175*, 519–530. [[CrossRef](#)]
206. Sophocleous, M.; Savva, P.; Petrou, M.F.; Atkinson, J.K.; Georgiou, J. A Durable Screen-Printed Sensor for In Situ and Real-time Monitoring of Concrete's Electrical Resistivity Suitable for Smart Buildings/Cities and IoT. *IEEE Sens. Lett.* **2018**, *2*, 1–4. [[CrossRef](#)]
207. Badr, J.; Fargier, Y.; Palma-Lopes, S.; Deby, F.; Balayssac, J.-P.; Delepine-Lesoille, S.; Cottineau, L.-M.; Villain, G. Design and Validation of a Multi-Electrode Embedded Sensor to Monitor Resistivity Profiles over Depth in Concrete. *Constr. Build. Mater.* **2019**, *223*, 310–321. [[CrossRef](#)]
208. Bourreau, L.; Bouteiller, V.; Schoefs, F.; Gaillet, L.; Thauvin, B.; Schneider, J.; Naar, S. Uncertainty Assessment of Concrete Electrical Resistivity Measurements on a Coastal Bridge. *Struct. Infrastruct. Eng.* **2019**, *15*, 443–453. [[CrossRef](#)]
209. Correia, S.F.H.; Antunes, P.; Pecoraro, E.; Lima, P.P.; Varum, H.; Carlos, L.D.; Ferreira, R.A.S.; André, P.S. Optical Fiber Relative Humidity Sensor Based on a Fbg with a Di-ureasil Coating. *Sensors* **2012**, *12*, 8847–8860. [[CrossRef](#)] [[PubMed](#)]
210. Liehr, S.; Breithaupt, M.; Krebber, K. Distributed Humidity Sensing in PMMA Optical Fibers at 500 nm and 650 nm Wavelengths. *Sensors* **2017**, *17*, 738. [[CrossRef](#)] [[PubMed](#)]
211. Chai, J.; Liu, Q.; Liu, J.; Zhang, D. Optical Fiber Sensors Based on Novel Polyimide for Humidity Monitoring of Building Materials. *Opt. Fiber Technol.* **2017**, *41*, 40–47. [[CrossRef](#)]
212. Moerman, W.; Taerwe, L.; Waele, W.D.; Degriek, J.; Baets, R. Application of Optical Fibre Sensors for Monitoring Civil Engineering Structures. *Struct. Concr.* **2015**, *2*, 63–71. [[CrossRef](#)]

213. Silva, K.; Silva, F.; Mahfoud, T.; Khelidj, A.; Brientin, A.; Azevedo, A.; Delgado, J.; de Lima, A. On the Use of Embedded Fiber Optic Sensors for Measuring Early-Age Strains in Concrete. *Sensors* **2021**, *21*, 4171. [[CrossRef](#)]
214. Fuhr, P.L.; Huston, D.R. Corrosion Detection in Reinforced Concrete Roadways and Bridges via Embedded Fiber Optic Sensors. *Smart Mater. Struct.* **1998**, *7*, 217–228. [[CrossRef](#)]
215. Domaneschi, M.; Cimellaro, G.; Ansari, F.; Morgese, M.; Inaudi, D. Embedded Fiber-Optic Sensors in Reinforced Concrete Elements of Bridge Structures. In *Bridge Maintenance, Safety, Management, Life-Cycle Sustainability and Innovations*; CRC Press: Boca Raton, FL, USA, 2021; pp. 1657–1664. [[CrossRef](#)]
216. Figueira, R.B.; Silva, C.J.R.; Pereira, E.V.; Salta, M.M. Alcohol-Aminosilicate Hybrid Coatings for Corrosion Protection of Galvanized Steel in Mortar. *J. Electrochem. Soc.* **2014**, *161*, C349–C362. [[CrossRef](#)]
217. Torres-Luque, M.; Bastidas-Arteaga, E.; Schoefs, F.; Sánchez-Silva, M.; Osma, J.F. Non-Destructive Methods for Measuring Chloride Ingress Into Concrete: State-of-the-art and Future Challenges. *Constr. Build. Mater.* **2014**, *68*, 68–81. [[CrossRef](#)]
218. Navarro, I.J.; Yepes, V.; Martí, J.V. Life Cycle Cost Assessment of Preventive Strategies Applied to Prestressed Concrete Bridges Exposed to Chlorides. *Sustainability* **2018**, *10*, 845. [[CrossRef](#)]
219. Kruschwitz, B. Optical Fiber Sensors for the Quantitative Measurement of Strain in Concrete Structures. In *Proceedings of the First European Conference on Smart Structures and Materials*; International Society for Optics and Photonics: Washington, DC, USA, 1992; Volume 1777, p. 17771E.
220. Lau, K.T.; Chan, C.C.; Zhou, L.-M.; Jin, W. Strain Monitoring in Composite-Strengthened Concrete Structures Using Optical Fibre Sensors. *Compos. Part B Eng.* **2001**, *32*, 33–45. [[CrossRef](#)]
221. Estella, J.; de Vicente, P.; Echeverría, J.C.; Garrido, J.J. A Fibre-Optic Humidity Sensor Based on a Porous Silica Xerogel Film as the Sensing Element. *Sens. Actuators B Chem.* **2010**, *149*, 122–128. [[CrossRef](#)]
222. Wang, Y.; Tjin, C.S.; Sun, X.; Lim, T.-K.; Moyo, P.; Brownjohn, J.M.W. Simultaneous Monitoring of Strain and Temperature in Concrete Structures with Embedded Fiber Bragg Gratings. In *Proceedings of the Second International Conference on Experimental Mechanics*; International Society for Optics and Photonics: Washington, DC, USA, 2001; Volume 4317, pp. 540–545.
223. Wong, A.C.; Childs, P.A.; Berndt, R.; Macken, T.; Peng, G.-D.; Gowripalan, N. Simultaneous Measurement of Shrinkage and Temperature of Reactive Powder Concrete at Early-Age Using Fibre Bragg Grating Sensors. *Cem. Concr. Compos.* **2007**, *29*, 490–497. [[CrossRef](#)]
224. Liu, Z.; Zhang, Z.F.; Tam, H.-Y.; Tao, X. Multifunctional Smart Optical Fibers: Materials, Fabrication, and Sensing Applications. *Photonics* **2019**, *6*, 48. [[CrossRef](#)]
225. Cusano, A.; Breglio, G.; Giordano, M.; Nicolais, L.; Cutolo, A. Multifunction Fiber Optic Sensing System for Smart Applications. *IEEE/ASME Trans. Mechatron.* **2004**, *9*, 40–49. [[CrossRef](#)]
226. Leung, C.K.Y.; Wan, K.T.; Chen, L. A Novel Optical Fiber Sensor for Steel Corrosion in Concrete Structures. *Sensors* **2008**, *8*, 1960–1976. [[CrossRef](#)] [[PubMed](#)]
227. Femenias, Y.S.; Angst, U.; Moro, F.; Elsener, B. Development of a Novel Methodology to Assess the Corrosion Threshold in Concrete Based on Simultaneous Monitoring of pH and Free Chloride Concentration. *Sensors* **2018**, *18*, 3101. [[CrossRef](#)] [[PubMed](#)]
228. Angst, U.M.; Elsener, B.; Larsen, C.K.; Vennesland, Ø. Chloride Induced Reinforcement Corrosion: Electrochemical Monitoring of Initiation Stage and Chloride Threshold Values. *Corros. Sci.* **2011**, *53*, 1451. [[CrossRef](#)]
229. Grattan, K.T.; Ning, Y.N. Optoelectronics, Imaging and Sensing. In *Optical Fiber Sensor Technology: Applications and Systems*; Grattan, L.S., Meggitt, B.T., Eds.; Springer: Berlin/Heidelberg, Germany, 1999; ISBN 978-0-412-82570-5.